A STUDY OF INTERFACIAL WAVES AND HEAT TRANSFER FOR TURBULENT CONDENSATION IN VERTICAL TUBES

by

Oscar Bryan Taliaferro, Jr.

Thesis submitted to the Graduate Faculty of the

Virginia Polytechnic Institute

in partial fulfillment of the requirements for the degree of

MASTER OF SCIENCE

in

Mechanical Engineering

APPROVED:

Dr. William P. Goss, Chairman

Dr. William C. Thomas

Dr. James B. Jones

April 1970

Blacksburg, Virginia

ACKNOWLEDGEMENTS

The author wishes to express his sincere appreciation to for his direction and guidance in this research project. Without his continuing enthusiasm, his willingness to discuss special problems as they arose, and his encouragement this work and this thesis would not have been possible. The author is also indebted to the men in the Mechanical Engineering Shop and to a work-study student, for their help in constructing the test facility. The author is extremely grateful to and for their efficient and cooperative efforts in typing this thesis. Appreciation is also expressed for the financial support received from the National Science Foundation and the National Aeronautics and Space Administration during the author's program of study. Finally, the author expresses deep graditude to his wife, , for her patience, understanding, and sacrifice which provided the real inspiration to begin and to complete this work.

TABLE OF CONTENTS

List of Figures

List of Tables

Nomenclature

A = cross-sectional flow area (ft^2)

a_i ($i = 0,1,2,...$) = coefficients of Chebyshev polynomials obtained in least squares fit

b_i ($i = 1,4$) = constants used in an entrainment correlation

c_p = specific heat (B/lbm-F)

D_i = inside diameter of the small pipe (in)

D_o = outside diameter of the small pipe (in)

f = wave contact frequency (sec^{-1})

g_c = dimensional constant (32.174 lbm-ft/lbf-sec^2)

H = specific enthalpy (B/lbm)

h = distance between tip of needle probe and pipe wall (in)

h_c = local condensing heat transfer coefficient (B/hr-ft^2-F)

H_o = stagnation specific enthalpy of steam entering the condenser (B/lbm)

J = energy conversion factor (778 ft-lbf/B)

K = constant used in entrainment correlation

k = thermal conductivity (B/hr-ft-F)

L = distance from steam entrance along the condenser (ft)

$Nu = h_c \delta / k_l$ = film Nusselt number

q = local heat flux based on inside diameter of pipe (B/hr-ft^2)

Q_t = rate of total heat removed (B/hr)

$R_{e_g} = \rho_g V_g (D_i - 2\delta)/\mu_g$ = gas Reynolds number

$R_{e_l} = \rho_l V_l \delta / \mu_l$ = liquid film Reynolds number

$R'_{e_g} = 4W_g/\pi D_i \mu_g$ = superficial gas Reynolds number

$R'_{e_l} = 4W_l/\pi D_i \mu_l$ = superficial liquid Reynolds number

s = dummy variable in entrainment correlation

T = temperature (F)

$\Delta T_f = (T_g - T_{iw})$ = temperature drop across the liquid film (F)

V = mean velocity (ft/sec)

V_w = wave velocity (ft/sec)

W = mass flow rate (lbm/hr)

x_D, x_0 = normalization constants used in Chebyshev polynomial curve fit

δ = film thickness (in)

δ_m = mean film thickness (in)

δ_{md} = modal film thickness (in)

δ_s = continuous liquid sublayer thickness (in)

δ_z = film thickness given by Zivi's correlation (in)

δ' = film disturbance layer (in)

$\theta = W_g/W_t$ = dynamic quality

μ = dynamic viscosity (lbm/ft-sec)

ρ = density (lbm/ft^3)

$\chi = W_g/(W_g + W_e)$ = entrainment quality

Subscripts

cu = copper

cw = cooling water

e = entrained liquid

g = gas in the steam core

iw = inside wall of the pipe

l = liquid film

ow = outside wall of the pipe

t = total

I. INTRODUCTION

At the present time the interaction of a slow moving liquid and a high speed gas and the resulting interfacial wave characteristics are not well understood. The generation of these interfacial waves occurs in external flows such as air movement across a body of water and in internal gas-liquid flows such as those found in tube condensers, tube evaporators, and oil-natural gas pipelines. These internal flows have been categorized into numerous flow regimes and a listing of these regimes is given by Bell, Taborek, and Fenoglio (1).

Of special interest in this study is the annular mist flow regime which occurs in the condensation of steam in a small vertical tube. Annular mist flow may be defined as the concurrent flow of a gas and a liquid in a circular duct with part of the liquid flowing in an annulus adjacent to the duct wall while the remainder flows entrained in the gaseous core. The present available methods for predicting the mass, momentum, and energy transfer for this two-phase flow problem are often inadequate. They usually rely on either a model requiring several simplifying assumptions, which are sometimes invalid, or a rough empirical correlation with limited applicability. The information currently available on the properties of the vapor-liquid interface and their effect on mass, momentum, and energy transfer is rather incomplete. A more thorough understanding of this problem could be derived from knowledge of the

behavior of the liquid film and the surface waves which usually occur in this type of flow. More specifically, information about the interfacial wave height, frequency, spacing, velocity, and the relations between these quantities and the dynamic flow parameters such as liquid and vapor Reynolds numbers and the heat transfer coefficients would be helpful.

The purpose of this investigation is to obtain this information.

II. SURVEY OF LITERATURE

In general, internal gas-liquid two-phase flows may be either diabatic where heat is exchanged with the surroundings or adiabatic. There also may be one or several components present. In single-component two-phase flows the gas and the liquid are of identical molecular species, while for two-component flows this is not the case.

For two-component flows such as air-water mixtures substantial literature on the interfacial properties is available. In an early study McManus (2) investigated film establishment, pressure drop, and film surface conditions for an adiabatic air-water flow. In an attempt to predict effects of various parameters on film dimensions he reported the film roughness, which is a measure of the wave height, to be dependent on film depth and gas and liquid flow rates.

Swanson (3) later studied the interfacial waves for an air-water mixture and found the average wave velocity to be roughly equal to the friction velocity of the gas. The friction velocity was taken to be the same as that for the gas flowing alone in the pipe. Swanson also found the average distance between waves to be a function of wave amplitude.

In an attempt to include wave effects in calculations a number of investigators (2, 4, and 5) have drawn the analogy between film roughness and equivalent pipe sand roughness. However, as

Lilleleht and Hanratty (4) have pointed out, the definition of equivalent sand roughness for gas-liquid interfaces is completely arbitrary and might bear little relation to the actual wave structure.

Pletcher and McManus (6) have investigated heat transfer in horizontal air-water flows. They found the local heat transfer coefficient to correlate with the gas Reynolds number for given liquid flow rates. This coefficient was calculated from the temperature drop across the liquid film and the heat flux which was determined from the power input to an electrically heated test section. Qualitatively, the heat transfer coefficient appeared to increase with gas Reynolds number until it reached some maximum after which it gradually decreased and converged to a value independent of both gas Reynolds number and liquid flow rate. In their study Pletcher and McManus did not investigate interfacial wave behavior.

For single-component diabatic two-phase flow the literature available is somewhat limited. This is true for several reasons. In this type of flow film behavior and mass, momentum, and energy transfer rates are affected by thermal as well as hydrodynamic phenomena. Furthermore, the mass, momentum, and energy exchanges between the gas and the liquid vary continuously along the flow, never reaching an equilibrium as in two-component flows. Consequently the precise determination of the pressure drop and of the liquid

and gas velocities and flow rates presents considerable difficulty. Nevertheless, several analytical and experimental studies have been conducted on the pressure drop and heat transfer in condensing flows. For a condensing vapor Soliman, Schuster, and Berenson (7) have developed an analytical means of predicting the heat transfer by including mass, momentum, and gravity effects. These terms were used to obtain an overall friction factor which, with the Prandtl number, was used to correlate the heat transfer coefficient. In their analysis the assumptions were made of a smooth vapor-liquid interface and no liquid entrainment. Both effects were absorbed by the Lockhart-Martinelli pressure parameter employed. The Lockhart-Martinelli correlation for prediction of pressure drop generally gives the best results of the most widely used pressure drop correlations as discussed by Dukler and Wicks (8). Nevertheless, this correlation often predicts pressure drop with an error as much as one hundred percent. Thus the use of this parameter which ignores the details of the flow pattern leaves much to be desired in the accurate prediction of the heat transfer coefficient.

Goodykoontz and Dorsch (9) have taken extensive data covering a wide range of heat transfer coefficients for high velocity condensation of steam and Freon in vertical tubes. A general correlation of the heat transfer coefficient and a gas mass flow parameter, $\theta(W_t/A_t)^2$, was obtained. This correlation was independent

of the pipe diameter. The heat transfer coefficient was shown to increase as this parameter increased. In addition, the pressure drop correlated in terms of common pipe friction parameters that included the flow rate, total condensing length, and specific volume of the vapor at the inlet. Neither of these correlations included film characteristics.

Robson and Hilding (10) made film measurements for steam condensing in a horizontal tube. Wave frequency and velocity measurements were taken at various circumferential positions at two different locations. Gas and liquid flow rates at these two locations were determined from an energy balance. No simultaneous measurements were made to determine the local heat transfer coefficients.

For the present investigation several techniques for measuring liquid film properties were considered. These methods are discussed by Collier and Hewitt (11) and by Bergles (12). Finally selected was the needle contact method where the difference between the electrical conductivity of the gas and of the liquid is used to detect the contact of the liquid film or of a wave with the tip of the needle probe. Its advantages are that wave amplitude can be determined fairly accurately, the probes can be easily constructed, and the required instrumentation is rather simple. Information as to the frequency, length, and velocity of the waves can also be obtained. However, as the needle contact probe is

merely an on-off switch, it gives no direct information as to the wave form.

Hilding and Robson (10) used two such probes positioned one half inch apart to determine wave velocity. Chien and Ibele (13) also used contact probes for a study of film thicknesses and pressure drops in an air-water mixture. As Chien and Ibele suggested, the experimental determination of the thickness of a wavy film is somewhat a matter of definition. Using needle contact probes, one may obtain two different but related measurements of film thickness. One, the modal film thickness, is defined as the distance between the probe tip and the tube wall where the frequency of wave contact with the probe is a maximum. The second, the mean film thickness, is the distance between the probe tip and the tube wall where the probe is in contact with gas and liquid for an equal amount of time. Unfortunately, it is difficult to ascertain which of these two methods gives the best figure to use in an analysis in which mean liquid and gas velocities are to be determined. Nevertheless, Chien and Ibele (13) have reported the two measurements to be in close agreement for a superficial liquid Reynolds number, R'_{e_1}, of 4000 for an air-water flow. For R'_{e_1} above this value mean thickness is larger than modal and for R'_{e_1} below, the reverse is true.

III. DESCRIPTION OF EQUIPMENT

A schematic diagram of the test facility used in this study is given in Figure 1. The facility consists primarily of the steam and the cooling water systems, the condenser, the test section, and the associated instrumentation.

The operation of this facility is described as follows. Steam from the building supply at 75 psig flows through a two-inch supply line to the plenum chamber, which is a cylindrical tank twelve inches in diameter and thirty inches long. Installed in this supply line are a valve to control plenum chamber pressure, a quick-acting ball valve for emergency shutdown, and a steam strainer. The steam then flows through the condenser and test section. The steam and condensate mixture leaving the test section is totally condensed and subcooled in the coil of three-quarter-inch copper tubing, thirty feet long, placed in the water bath. Subcooling the condensate reduces evaporation losses at the weigh tank, which is used to determine the steam flow rate. The cooling water system includes a surge tank which contains an air cushion to dampen pressure fluctuations. The water, which enters this tank first, exits to the condenser through piping which permits either parallel flow or counterflow. The flow rate of the cooling water is also determined by a weigh tank.

Figure 2 gives the details of the condenser and test section, showing locations for the pressure taps, wall thermocouples, cooling water thermocouples, and the needle probes. A two-inch by three-

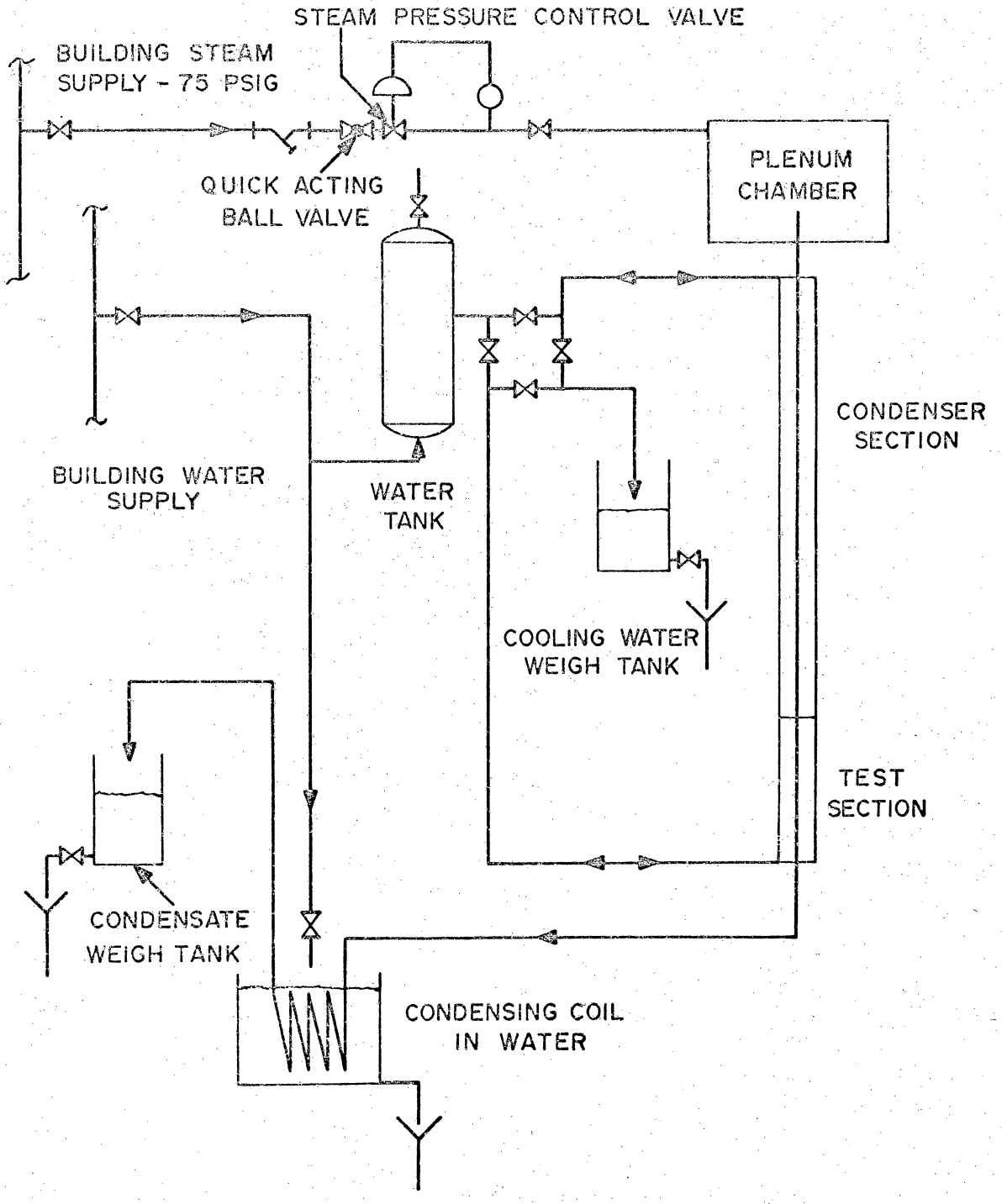

FIGURE 1 SCHEMATIC OF FACILITY

quarter-inch reducing nozzle, which is nine inches long, provides a smooth entrance of the steam into the condenser. The end of the nozzle which is in the plenum chamber is recessed three and one-half inches, as shown in Figure 2, to minimize the amount of condensate entering the condenser.

The condenser and test section consist primarily of two concentric copper pipes. Concentricity in the condenser is maintained by spacer rings as shown in the figure. During construction the pipes were cleaned to insure uniform surface conditions. The outsides were sandblasted and the inside of the small tube was cleaned with a rotating steel brush. The resulting surface was smooth to the touch. An expansion bellows allows relative movement between the two pipes. The test section is fastened to the condenser with steel flanges fabricated so that water and steam flow continuously through the annulus and small pipe respectively. Care was taken to see that the inside pipes of the two sections were flush when joined together, minimizing film disturbances caused by the joint. The test section was designed so that it could be easily disassembled for future modifications.

Details of the installation of the pressure taps, wall thermocouples, and cooling water thermocouples are shown in Figure 3. The loop in the stainless steel pressure tap tubing accommodates radial thermal expansion of the tubing itself and relative axial thermal expansion of the two copper pipes. Lines of one-quarter-inch copper

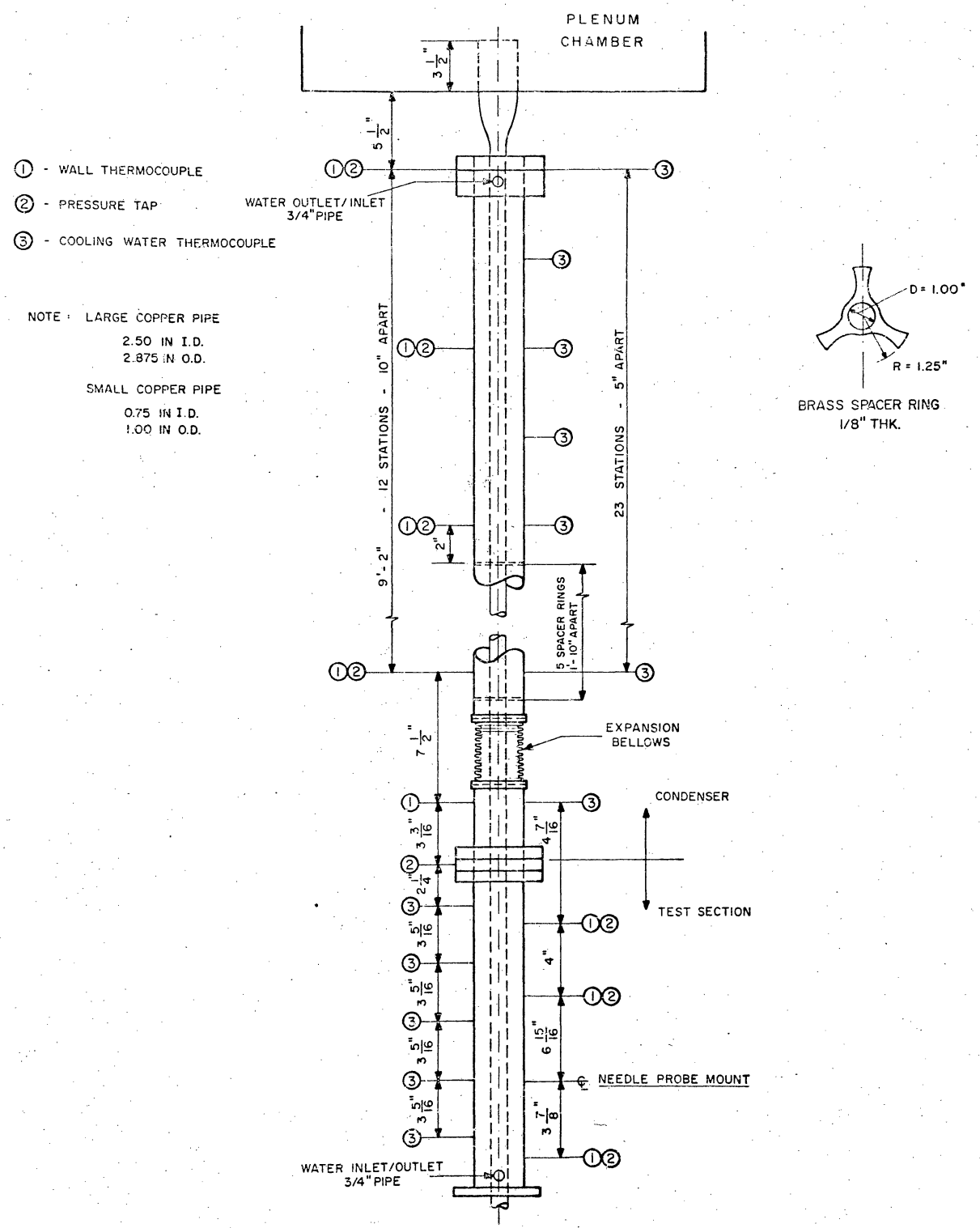

FIGURE 2 CONDENSER AND TEST SECTION

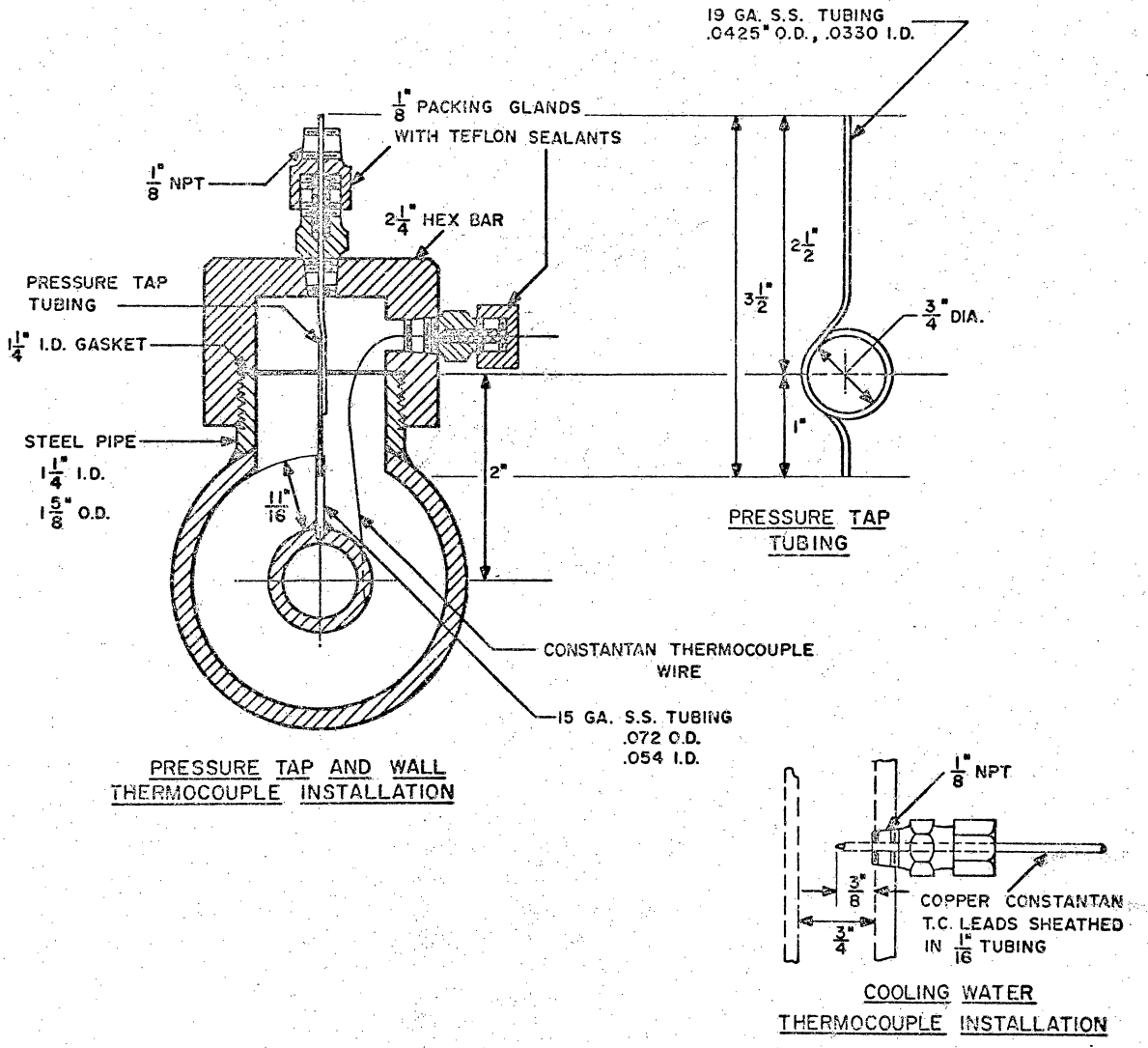

FIGURE 3 DETAILS OF PRESSURE TAP, WALL THERMOCOUPLE AND COOLING WATER THERMOCOUPLE INSTALLATIONS

refrigeration tubing connect the sealing glands for the pressure taps to the sixteen mercury manometers used to determine the steam pressures. The manometers were connected so that each one measured the pressure difference between two successive points. A Heise bourdon tube gage (range 0-250 psig; least count 0.5 psi) was connected to the plenum chamber and an identical gage connected to the lowest tap on the test section to give a reference for the manometers. The pressure lines were arranged so that air could be bled from them.

The outside wall temperatures along the smaller pipe were measured by copper-constantan thermocouples, the copper conductor being the copper pipe itself. For the installation of one of these thermocouples (see Figure 3) a 0.025 inch diameter hole was drilled tangent to the tube radius through the one-eighth-inch pipe wall. The 30 AWG constantan wire insulated with Kapton was inserted and the exposed tip soldered flush with the outside wall. This installation minimized heat conduction along the wire away from the thermocouple junction. Kapton insulation was chosen for its excellent abrasion and moisture resistance properties and for its high temperature rating.

A detail of the cooling water thermocouple installation is also given in Figure 3. These thermocouples are copper-constantan with an exposed junction. The leads are sheathed in a one-sixteenth-inch stainless steel tube, six inches long, and connected to a plug terminal. Two, twenty-four-point recording potentiometers were

connected to the twenty-nine cooling water thermocouples, and to a thermocouple located in the plenum chamber. An ice bath was used as a reference temperature. Before use these instruments were calibrated using a standard voltage source. In addition, the wall and cooling water thermocouples were checked at three different temperatures for accuracy. The temperatures used for this calibration check were that of cold water at 60 F, room temperature, and saturated steam near 60 psia. The instrumentation discussed here provided a full knowledge of conditions in the test section.

For measuring film properties two needle contact probes mounted in machine screws were fastened one half inch apart on a movable rectangular piston as shown in Figure 4. This piston was placed in a Plexiglas (methyl methacrylate) mount which was secured to the test section. This mount also held in place the micrometer (range 0-1 inch; least count 0.0001 inch) which was used for determining the probe position. Compression springs, though not shown in the figure, were placed in front of the piston to hold it firmly against the micrometer shaft. Also not shown are four teflon plugs which were embedded in one side of the piston to reduce the clearance between the piston and the rigid Plexiglas mount. This avoided any excess motion of the piston as it was moved back and forth by the micrometer. The mount was designed so that the elastic deflection of the Plexiglas caused by thrust forces of the micrometer shaft acting against the spring forces did not cause significant error in the determination of the probe position.

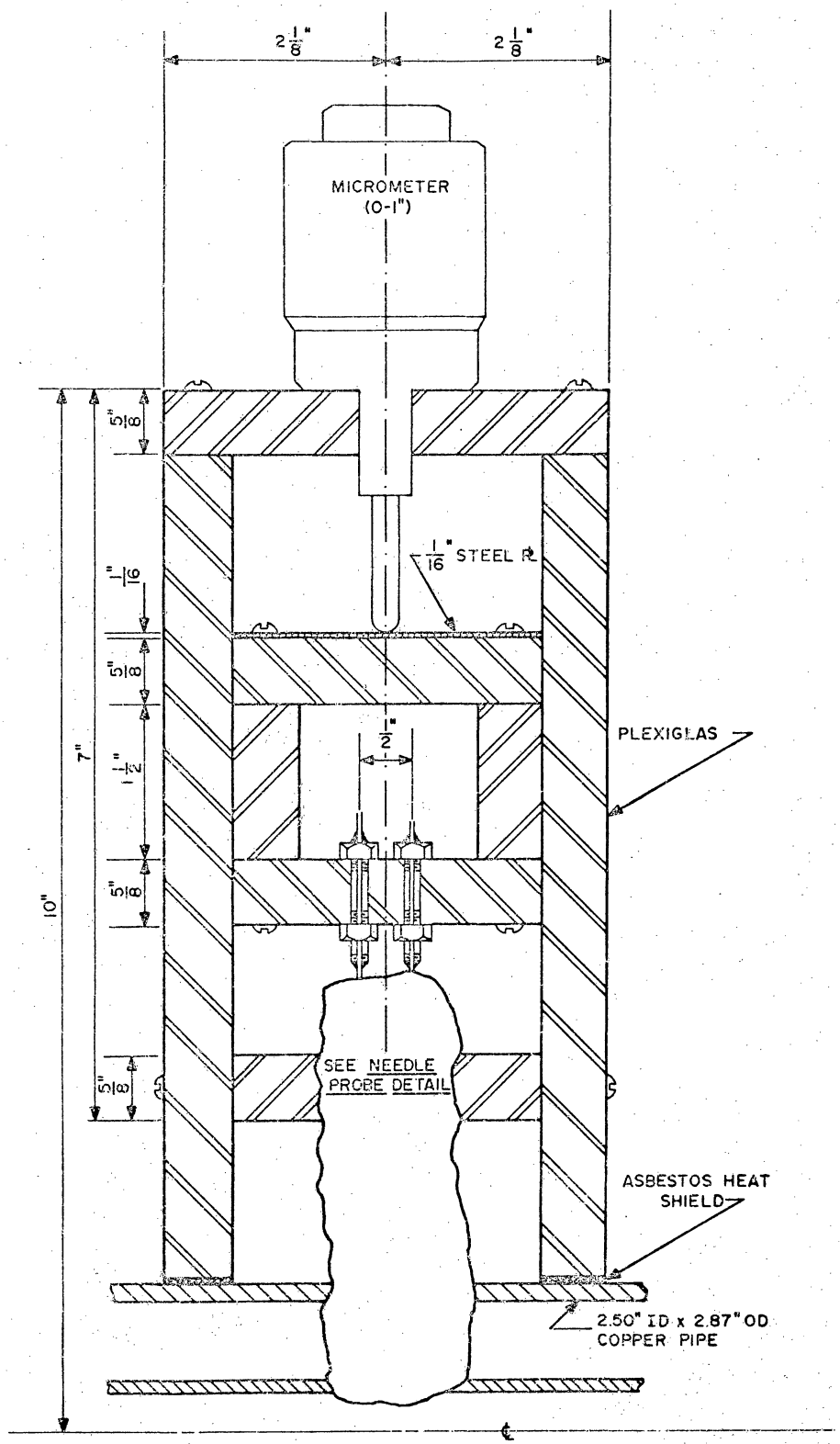

FIGURE 4 NEEDLE PROBE MOUNT

Details of the needle probes, seals, and entry ports into the small pipe are shown in Figure 5. The probes were made from thirty AWG insulated iron wire sheathed in six-inch long, 0.0425-inch O.D. by 0.027-inch I.D., stainless steel tubes. Each end of the probe was sealed with epoxy. The wire at the contact end protruded approximately one sixty-fourth of an inch from the epoxy and was sharpened to a point. (Most of the data were taken with this type probe. Afterwards a probe with a blunt end was tested and the signal characteristics were compared with those of the probe with a pointed tip. Results of this comparison are discussed in a later section.) The probes were sealed with one-sixteenth-inch NPT packing glands with re-usable teflon sealants. These glands were tightened just enough to provide an adequate pressure seal and yet permit probe movement. The probe tips were placed behind each other with respect to the steam flow direction and at the same position relative to the pipe wall.

The instrumentation and the probe circuit employed in obtaining film data are shown in Figure 6. The circuit was arranged so that the electrical potentials between the two needle probes and the pipe wall provided the input signals to the two channels on the oscilloscope (Tektronix type 564 storage oscilloscope, dual trace.) The potential between the upstream probe and the wall was the input signal for the electronic counter (Hewlett-Packard type 5233L). The microammeter was connected to measure the actual current flow in

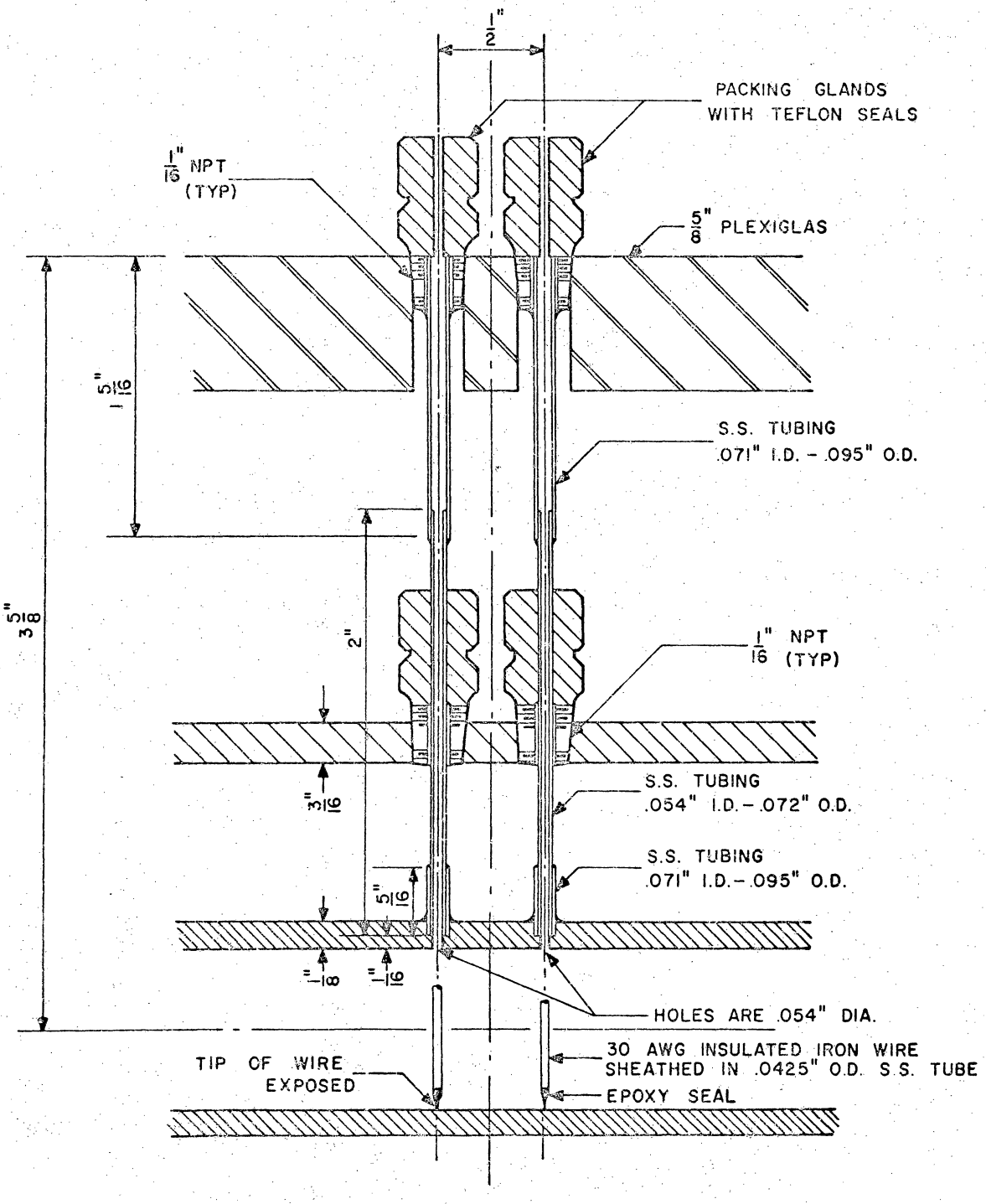

FIGURE 5 NEEDLE PROBE DETAIL

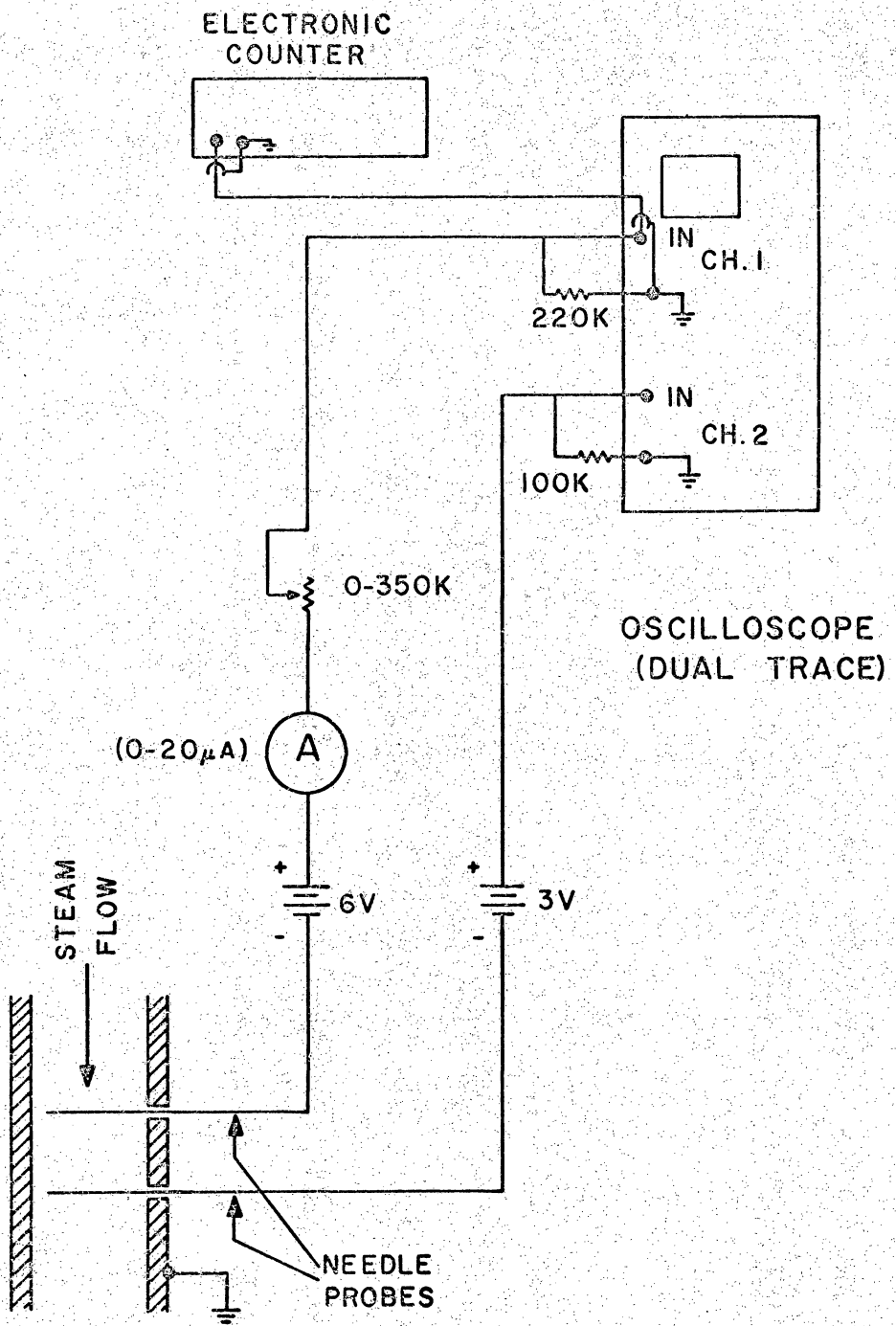

FIGURE 6 INSTRUMENTATION CIRCUIT FOR TEST SECTION

the circuit (i.e., between the upstream probe and the pipe wall). Two D.C. batteries were used as the power sources shown on the circuit diagram.

Photographs showing the test facility and a close-up of the test section are given in Figures 7 and 8.

The techniques employed in using the instrumentation described above to obtain film and heat transfer data are detailed in the following section.

Figure 7 Photograph of Test Facility

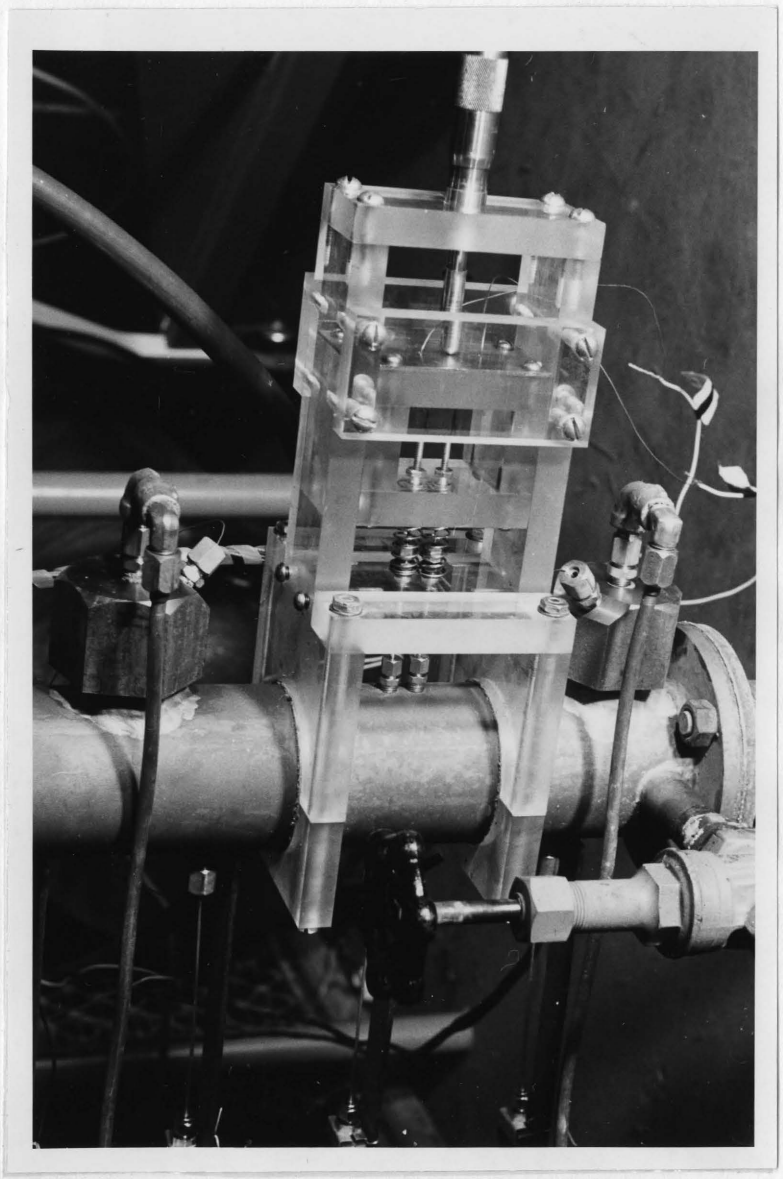

Figure 8 Close-Up of Test Section

IV. EXPERIMENTAL TECHNIQUE

Prior to facility start-up air in the pressure lines was eliminated by filling the small pipe with water at 60 psig and bleeding the pressure lines. When all the air had been removed, each manometer indicated a zero pressure differential, since the hydrostatic difference between two taps on the condenser was equalized by the hydrostatic difference in the pressure lines. When this task was completed the plenum chamber was allowed to come to atmospheric pressure and the bourdon tube gage zeroed at this pressure. At the same time the gage for the lowest pressure tap was zeroed and readings later adjusted to account for hydrostatic pressure differences. By observing the barometric pressure, the absolute pressures in the plenum chamber and at points along the condenser could be determined.

After the cooling water was made to flow in the annulus between the two pipes, the steam was turned on with water occupying the plenum chamber and the condenser tube. The throttling valve at the condensate weigh tank was then opened to permit release of the water and subsequent flow of the steam. Since steady state conditions were required, the facility was operated approximately an hour before obtaining any data.

To vary flow and heat transfer conditions in the condenser and test section, the pressure in the plenum chamber was set and then maintained by the pressure control valve. For each setting

of the plenum chamber pressure, several cooling water flow rates were selected by adjusting the throttling valve at the cooling water weigh tank. Furthermore, for each water flow rate the throttling valve at the condensate weigh tank was moved to several different positions to give different steam flow rates. Both the condensate and steam flow rates were determined by the weigh tank method. Before the data for a given set of conditions were obtained, the plenum chamber was drained of trapped condensate.

For the film measurements, the needle probes were initially positioned in the steam core and then traversed across the liquid film toward the pipe wall. This movement was accomplished by advancing the micrometer, thereby moving the piston on which the probes were mounted. During this process readings for wave velocity, wave frequency, and relative contact time for each run were taken at approximately fifteen different positions of the probes. At each position of the probes in the film and also that position at which the probes first touched the pipe wall the micrometer setting was noted. The point at which the probes touched the wall was easily determined, since the current flow in the ammeter suddenly increased and the signal on the oscilloscope reached that of ground. This last micrometer reading was subtracted from the readings for the previous various probe positions to give the distances between probe tip and pipe wall.

As the probes advanced toward the wall, intermittent contact with the waves on the liquid film was made. Since the electrical conductivity of a liquid is greater than that of its vapor, the wave contact with the probe caused a measurable drop in voltage between the probes and the wall. This voltage change during contact could be detected on the oscilloscope and with the electronic counter.

The counter was used to give the wave frequency of the upstream probe. Each time a wave contacted the tip the voltage between the probe and the wall changed and a single count was displayed on the counter. Counts were averaged over five counting periods of ten seconds each, giving frequency in counts per second. It was noted that at a given probe position the average for one ten-second period varied at the most five percent from the average for the five periods. Unfortunately, it was occasionally necessary to replace a probe which had short-circuited or had lost the epoxy seal at the tip. It was rather difficult to make all probes identical and, therefore, replacements altered the resistivity of the total circuit. Since the contact frequency depended on the counting level (i.e., the voltage change below which the counter would not register) the level was arbitrarily set before each run at a voltage midway between that when the probe was in the gas and when the probe tip was continuously submerged in the film. This step was taken to reduce dependence of wave frequency on probe characteristics.

To determine the relative contact time of the waves, the microammeter in the circuit was used. For each run the total deflection was taken as the difference between the two readings on the ammeter, one for which the upstream probe was positioned in the steam core and the other for which it was submerged in the liquid film. The relative contact time was taken to be the percentage of this total deflection indicated by the ammeter for a given probe position, a procedure used by McManus (2), and Chien and Ibele (13).

In obtaining wave velocities for a given probe position the oscilloscope was set to display and store a single sweep of the two probe signals. The traces displayed indicated the voltage changes which occurred when a moving wave passed by the two probes. The wave first contacted the upstream probe and a moment later the downstream probe. This resulted in a horizontal displacement of the two contact signals shown on the screen. By noting this displacement and the sweep rate of the oscilloscope the time required for a wave to travel the distance between the probes could be determined. While obtaining this information on wave velocity it was often necessary to display and erase a signal several times until a sharp, easily read trace was produced. At each probe position, this entire procedure was repeated several times in order to obtain the average wave velocity for that point. For probe positions below the modal film thickness, the probe signals could not be deciphered to give wave velocities. This difficulty

is explained by contact hysteresis. At these lower probe positions water from a passing wave tended to cling to the probe tip and before contact could be broken another wave passed by.

Several photographs of the oscilloscope patterns were taken during the investigation and two are given in Figure 9. Probe contact with the waves and the displacement of these contact signals can be easily observed. For this study twenty-four runs, designated with consecutive numbers from thirteen through thirty-six, were made. For the first twenty the cooling water was flowing upward (counter-flow) and for the last four, downward (parallel flow). The results are given in a later section.

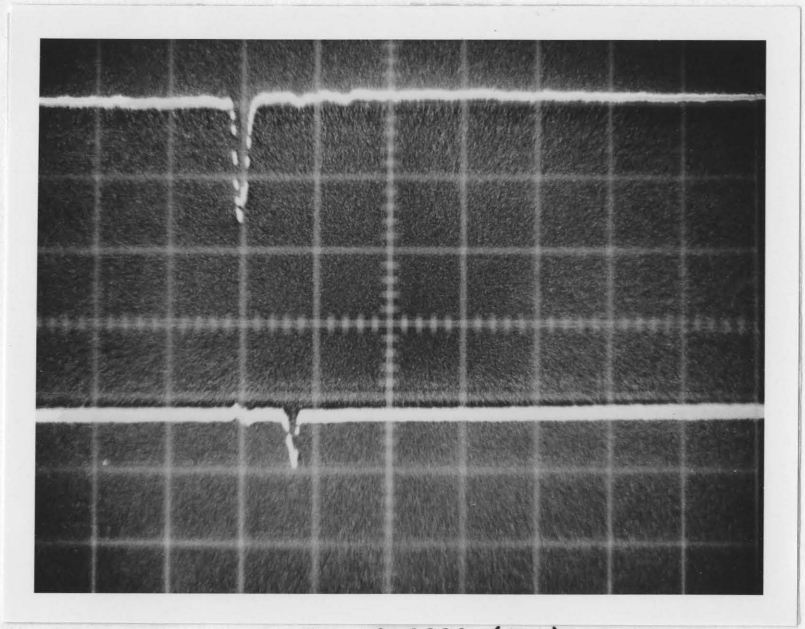

h = 0.0090 (in.)

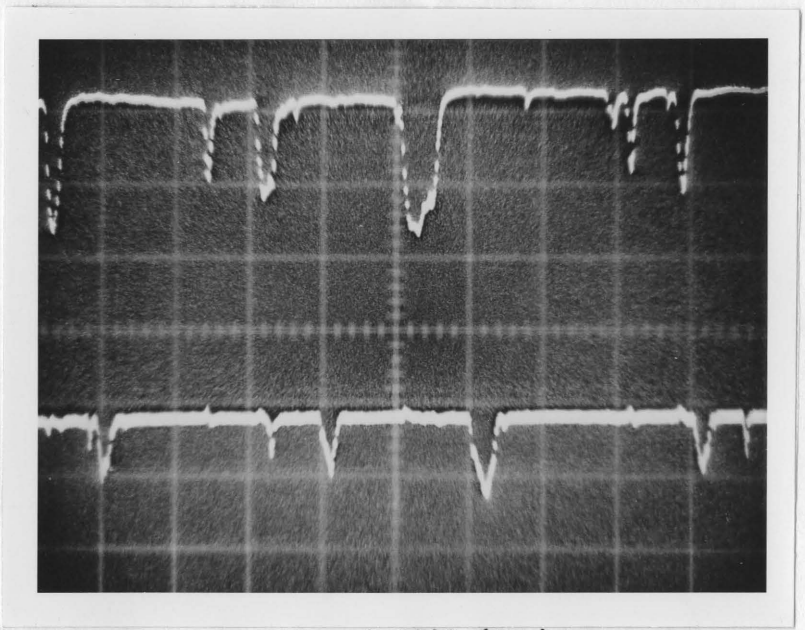

h = 0.0040 (in.)

Figure 9 Oscilloscope Traces for Two Probe Positions

V. ANALYSIS OF EXPERIMENTAL DATA

In the analysis of the experimental data obtained in this investigation the following assumptions were made about the condensing flow.

1. All conditions are time invariant.
2. Conditions about the pipe centerline are axisymmetric.
3. Axial heat conduction effects are negligible.
4. Body forces are negligible.
5. The temperature of the steam at the interface is the saturation temperature corresponding to the local static pressure.
6. Thermodynamic and transport properties of the liquid and gas are those at saturation.
7. There was no heat transfer to the surroundings.
8. The measured change in cooling water temperature equals the change in the bulk temperature of the cooling water.

The data taken in this investigation generally fall into two categories, that for the heat transfer and that for the liquid film. In this analysis curves were fitted to the data for static pressure, wall temperature, and cooling water temperature as a function of the axial distance along the condenser and the test section (Appendix A). From these curves the local heat flux and the local heat

transfer coefficient at the needle probes were determined (Appendix B). In addition, fitted curves were obtained for the wave frequency and the relative contact time from which the mean and modal film thicknesses were obtained. For each thickness the gas and liquid flow areas were computed. These areas along with the heat transfer information were used in an energy balance to determine the gas and liquid mean velocities, flow rates, and several other local parameters at the probes. These parameters are the gas and liquid Reynolds numbers, the superficial gas and liquid Reynolds numbers, the film Nusselt number, and the dynamic quality. The details of all these calculations are presented in Appendix B and the results are given in Tables BII and BIII.

Finally, several parameters describing the film surface were determined. These are the thickness of the continuous liquid sublayer, the disturbance layer thickness or wave amplitude, and the ratio of the difference between the mean film thickness and the sublayer thickness to the wave amplitude. These parameters for each run are given in Table BIV.

VI. RESULTS AND DISCUSSION

In this study a large amount of experimental data was obtained and many were of a statistical nature. Consequently, all the relationships inherent in these data are by no means exhausted in this discussion. Rather, several important correlations were derived and these are discussed.

A. Heat Transfer Results

The typical results of the axial temperature profiles of the saturated steam, the outside wall, and the cooling water for conditions of counter flow are shown in Figure 10. The results are similar for conditions of parallel flow except that the slope of the axial cooling water temperature variation is reversed. The temperature profile of the steam simply reflects the behavior of the static pressure since saturation conditions were assumed. The slope is negative since the pressure drop from frictional losses is greater than the rise from momentum recovery. This slope decreases slightly over the condenser length as the difference between these two decreases. Goodykoontz and Dorsch (9) report this effect and actually show a static pressure rise near the total condensing length. Total condensing was not achieved in this investigation, and such a pressure rise was not realized. The slope of the axial cooling water temperature variation for

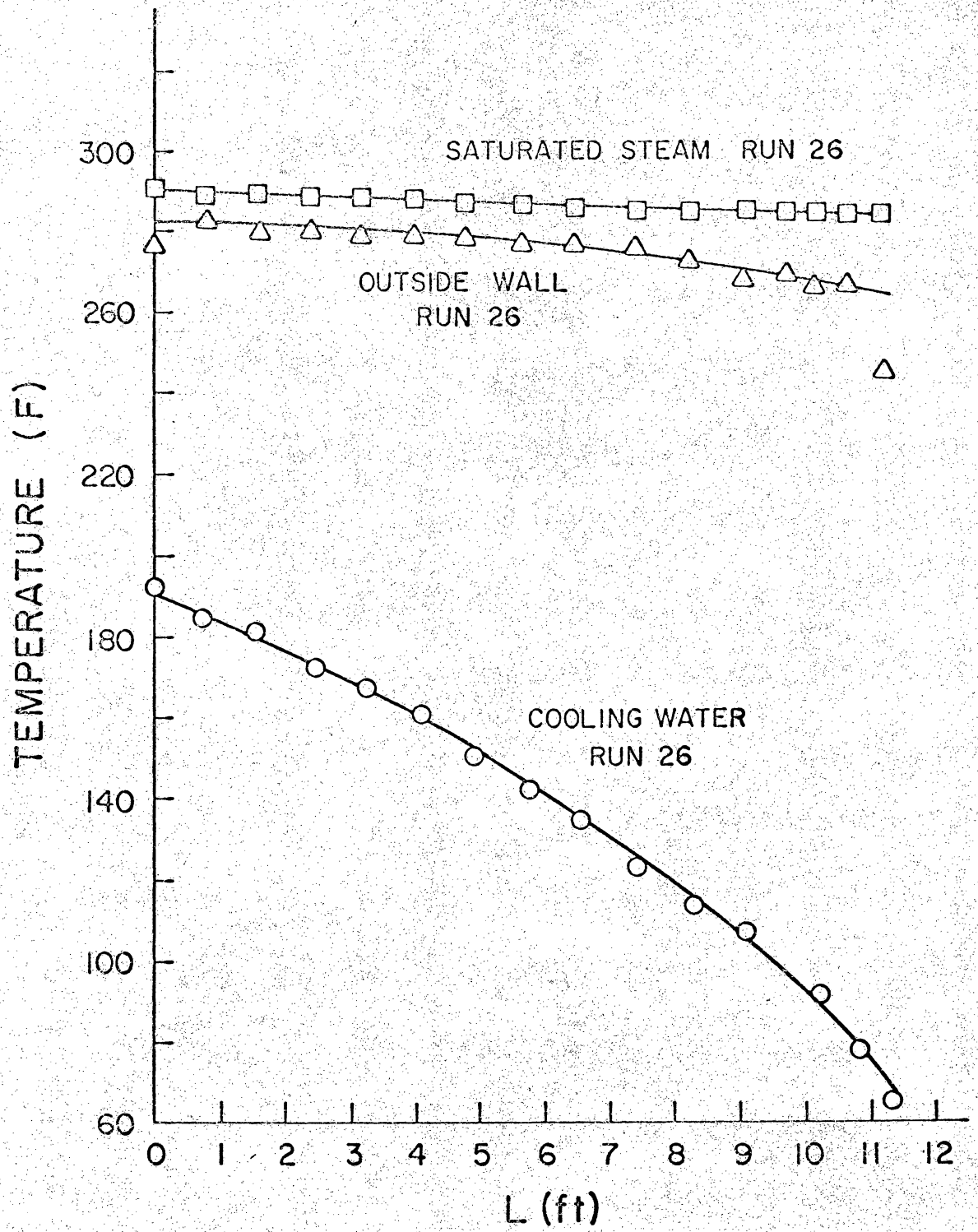

FIG. 10 TYPICAL AXIAL TEMPERATURE PROFILES

the run shown in the figure actually increases. This increase is less for higher rates of water flow. The experimental data for the static pressures and temperatures of the cooling water and the outside wall are given in Tables CI through CIII.

The axial variation of the local heat transfer coefficient and the local heat flux is shown in Figure 11. The heat flux, which is directly proportional to the slope of the axial cooling water temperature profile (Appendix B), increased over the condenser length at a constant rate. The local heat transfer coefficient, influenced strongly by the heat flux, increased at first and then decreased further down the tube. The decrease resulted from the increasing thermal resistance across the growing liquid film. The maximum heat transfer coefficient for most runs occurred about four to six feet from the steam entrance. These results are similar to trends observed by Goodykoontz and Dorsch (9). The heat transfer coefficients at the needle probes, which are of special concern in this study, ranged from 2214 to 5401 ($B/hr\text{-}ft^2\text{-}F$). All computed values of the local heat transfer coefficient and the local heat flux are given in Table BI.

B. Results of Film Measurements

The experimental data from the measurements of the liquid film are given in Table CIV. These measurements were wave contact frequency, relative contact time, and wave velocity for various

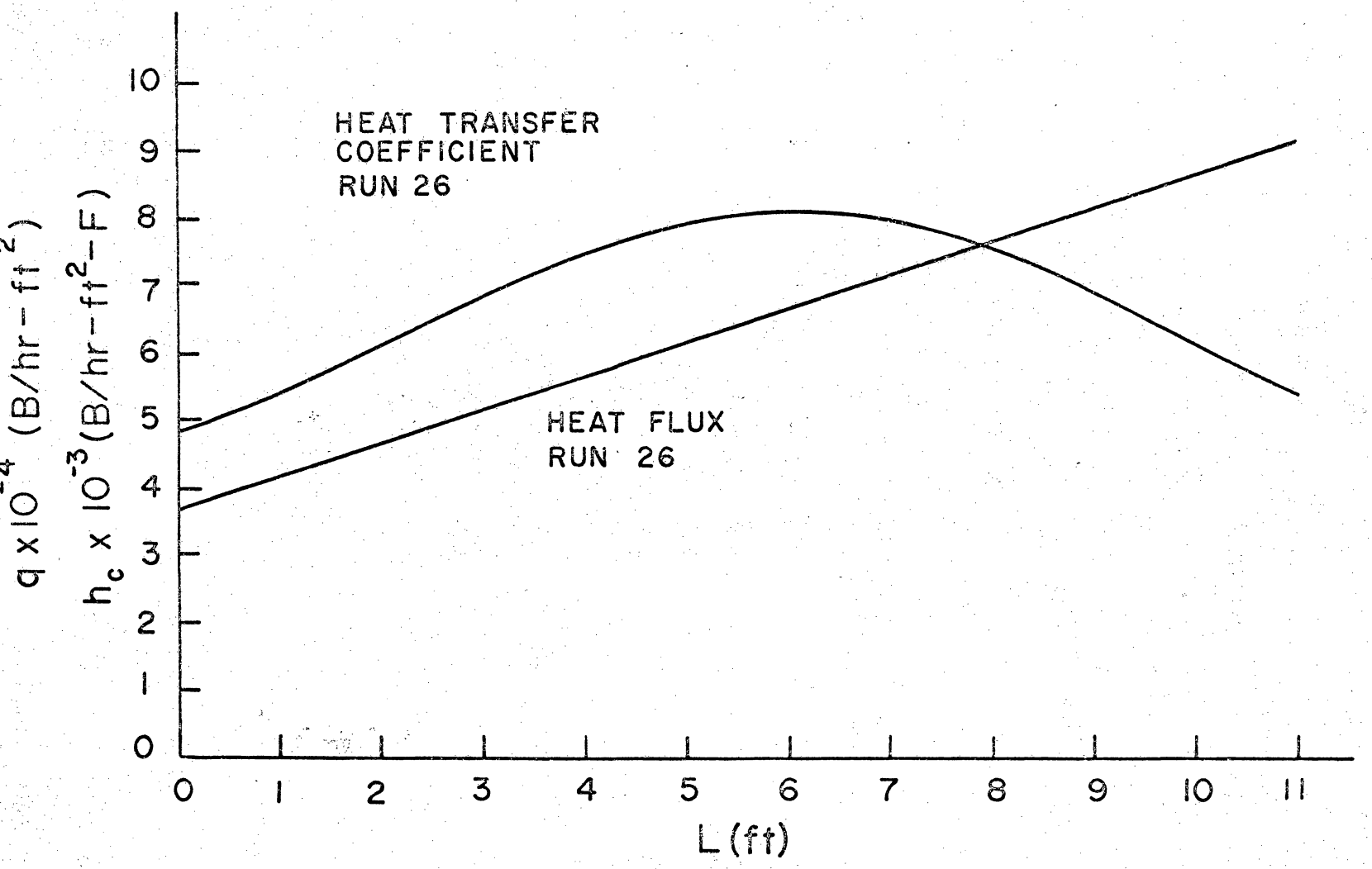

FIG 11 TYPICAL AXIAL VARIATION OF LOCAL HEAT FLUX AND LOCAL HEAT TRANSFER COEFFICIENT

probe positions. Typical results of the measurement of relative contact time and wave frequency are given in Figures 12 and 13. As these two figures indicate, the dynamic quality strongly influenced these measurements. Collier and Hewitt (11) show similar results for an upward flow of air and water in a one and one-quarter inch diameter pipe. However, for the same qualities these investigators reported film thicknesses generally greater than those obtained in this study. This difference results from several factors. Among these are the different pipe diameters, the opposite flow directions, and the dissimilarities between air-water flows and condensing flows.

A more relevant comparison would be that of the present film measurements with the prediction of film thickness given by Zivi's correlation. Zivi (14) has derived an analytical expression for the void fraction of a condensing vapor using the principle of minimum entropy production. From this correlation, assuming no liquid entrainment, a characteristic film thickness can be easily derived and is given as

$$\delta_z = \frac{D_i}{2} - \frac{D_i}{2}\left[\frac{1}{1 + \frac{(1-\theta)}{\theta}\left(\rho_g/\rho_l\right)^{2/3}}\right]^{1/2} . \qquad (1)$$

A comparison of the two measured film thicknesses with that given by Zivi's correlation is given in Figures 14 and 15. In most cases Eq. (1) gives a higher value than either measured value except

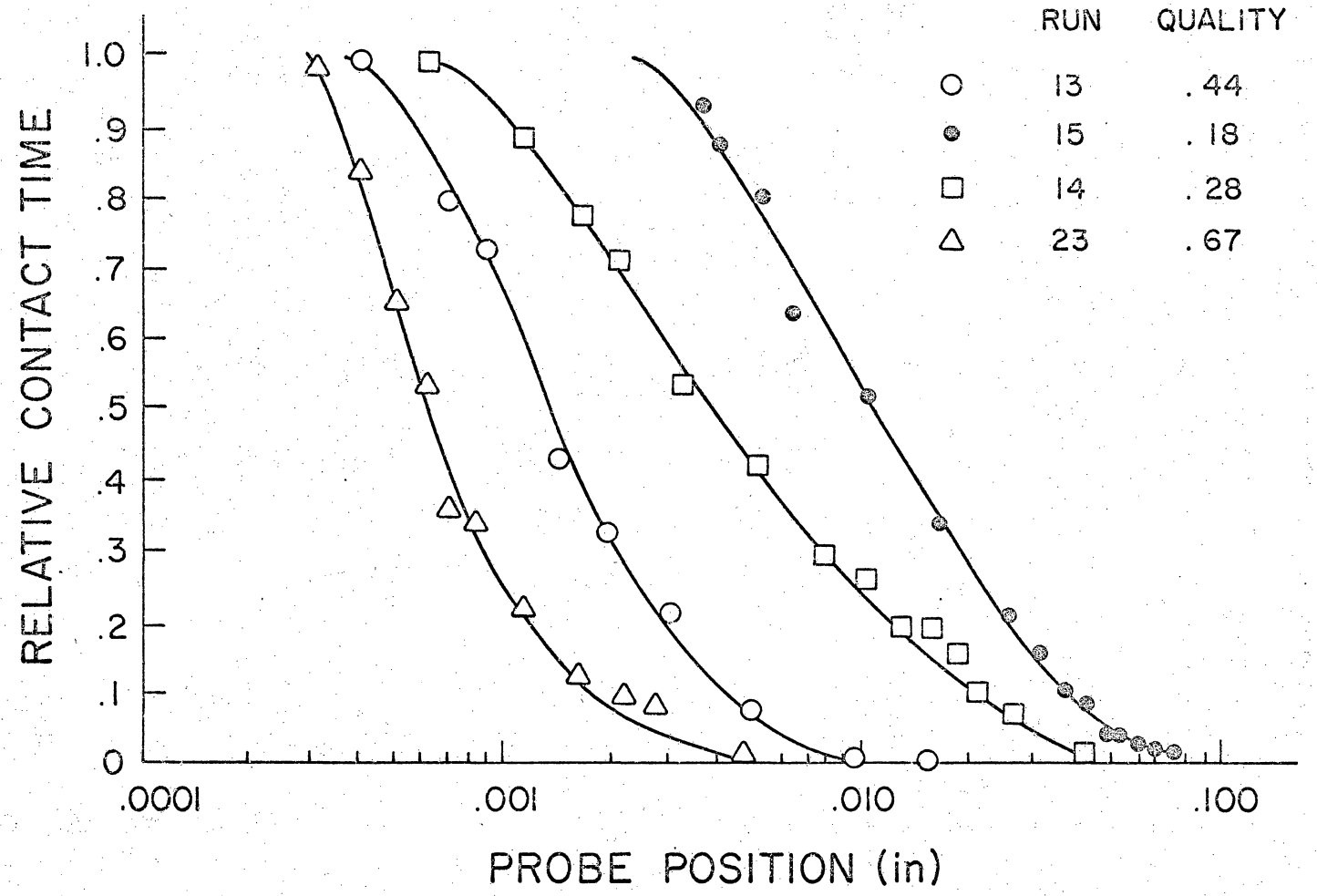

FIG. 12 RELATIVE CONTACT TIME OVER THE DISTURBANCE LAYER FOR SEVERAL QUALITIES

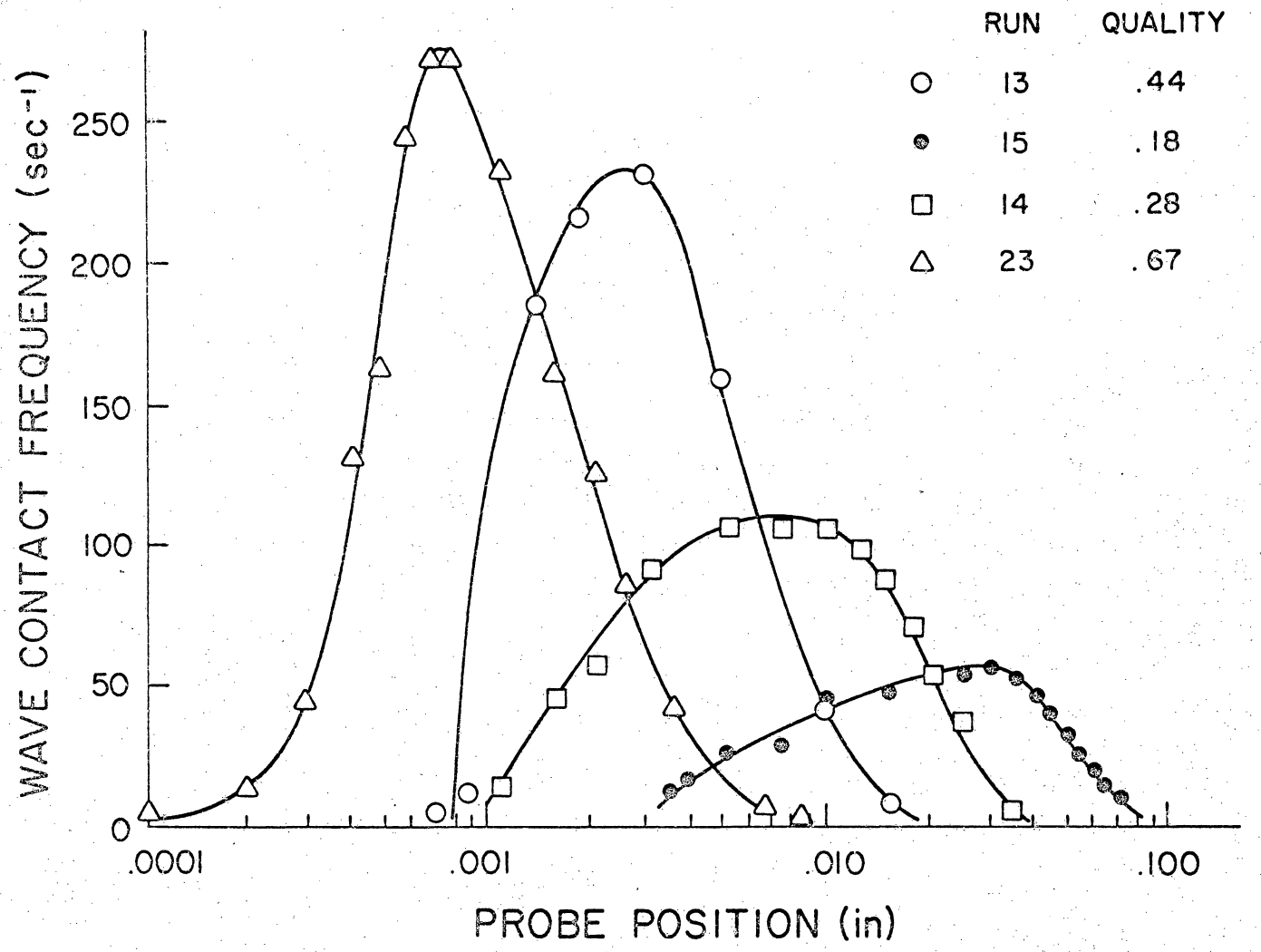

FIG. 13 WAVE CONTACT FREQUENCY OVER THE DISTURBANCE LAYER FOR SEVERAL QUALITIES

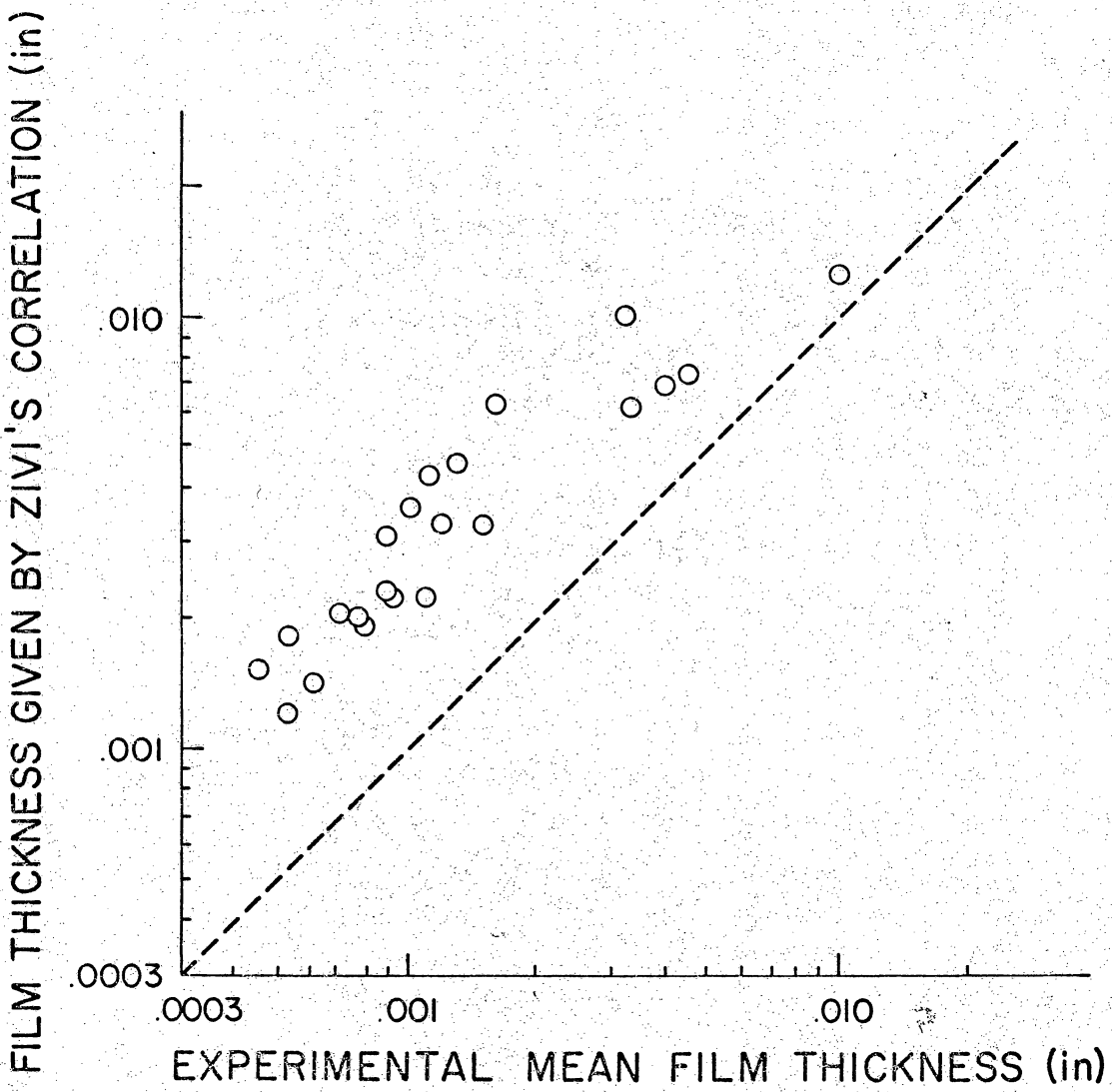

FIG. 14 COMPARISON OF EXPERIMENTAL MEAN FILM THICKNESS AND THAT GIVEN BY ZIVI'S CORRELATION

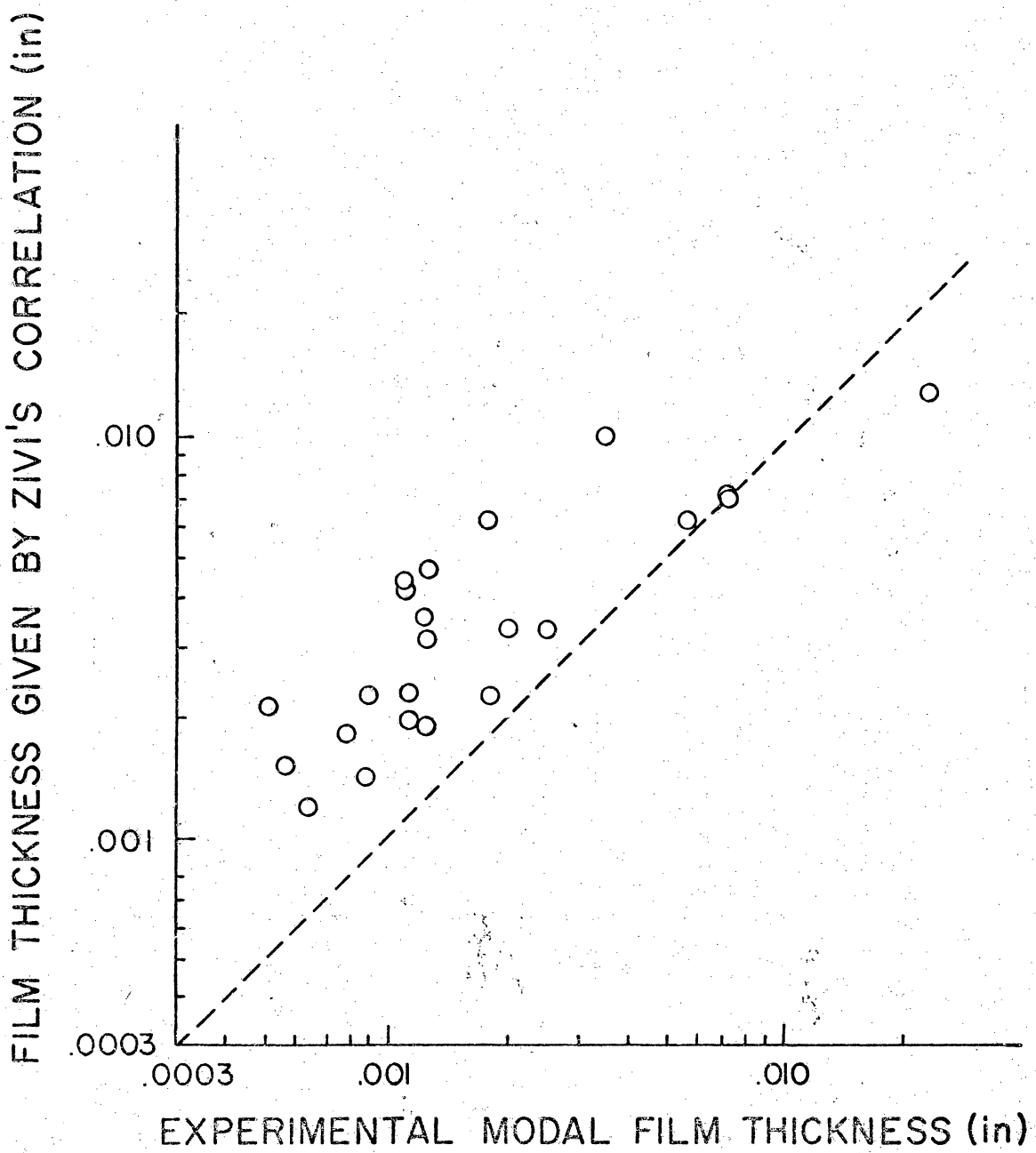

FIG. 15 COMPARISON OF MODAL FILM THICKNESS WITH THAT GIVEN BY ZIVI'S CORRELATION

at lower qualities where the modal film thickness agrees with Eq. (1) rather well.

A comparison of the two measured film thicknesses is shown in Figure 16. In most runs the modal film thickness was higher than the mean thickness. This fact contradicts the relation between these two for $R'_{e_1} > 4000$ which was suggested by Chien and Ibele (13) for an air-water flow. For all twenty-four runs made in this study the superficial liquid Reynolds number at the probes was above 4000, ranging from 5840 to 19100. Furthermore, no criterion for determining the relative magnitudes of these two measurements was indicated by any of the data.

The wave velocity measurements did not vary significantly over the liquid layer. Roll waves, waves with a crest velocity higher than the trough velocity, which are normally present in this type of flow, were not detected experimentally. This fact is a result of the shape of the needle probes. The dimensions of the exposed, pointed tip were of the same order of magnitude as those of the wave amplitude. As the probes moved through the film the wave crest was probably the first portion of the wave to make contact for each probe position.

C. Correlations

The film measurements yielded several significant functional relationships. First, the thickness of the disturbance layer, the

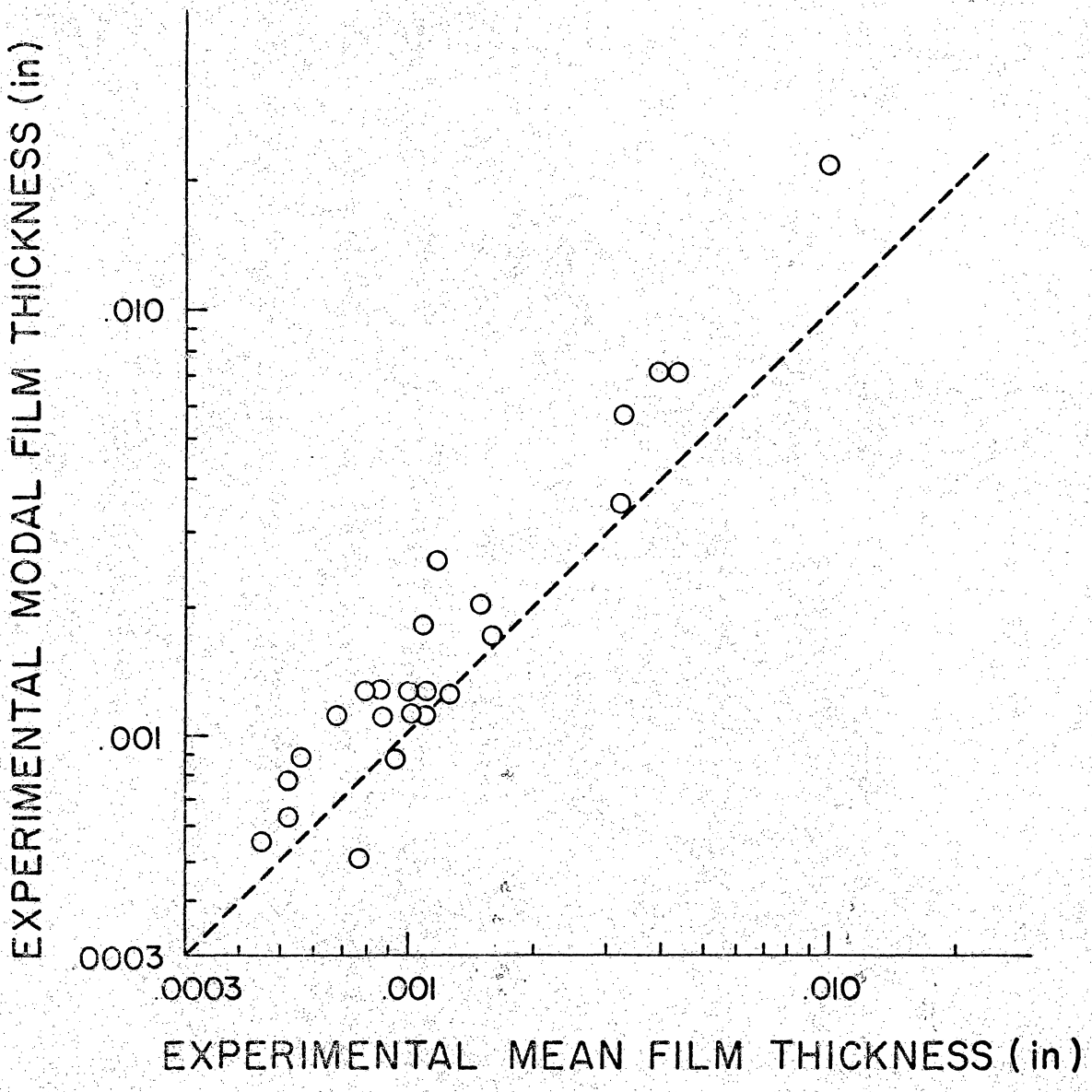

FIG. 16 COMPARISON OF MODAL AND MEAN FILM THICKNESS MEASUREMENTS

distance between the wave crest and trough, was dependent on the dynamic quality. It decreased with increasing quality as shown in Figure 17.

The actual surface of the film appears to be quite random in nature. The waves themselves vary in size and shape for a given set of conditions. Nevertheless, a statistical wave form has been derived which gives some insight into the gas-liquid interaction. This form is simply a time averaged shape of the waves and was determined from the wave frequency, relative contact time, and wave velocity data. A constant velocity equal to the average measured wave velocity was assumed over the disturbance layer. The analysis, which gives this statistical wave form is detailed in Appendix D and the results are given in Table DI.

The statistical wave form as shown in Figure 18 for several runs is very sharply peaked and has a relatively narrow base. Certainly an actual wave with such proportions could survive only momentarily in a real flow, since it would be broken up rapidly by the higher velocity gas. It is, therefore, reasoned that the film surface is in a continuous state of transience with waves being formed and almost instantly destroyed.

An attempt was made to find, by graphical integration, a characteristic film thickness from this statistical wave form. The ordinate on the graph, above and below which there was an

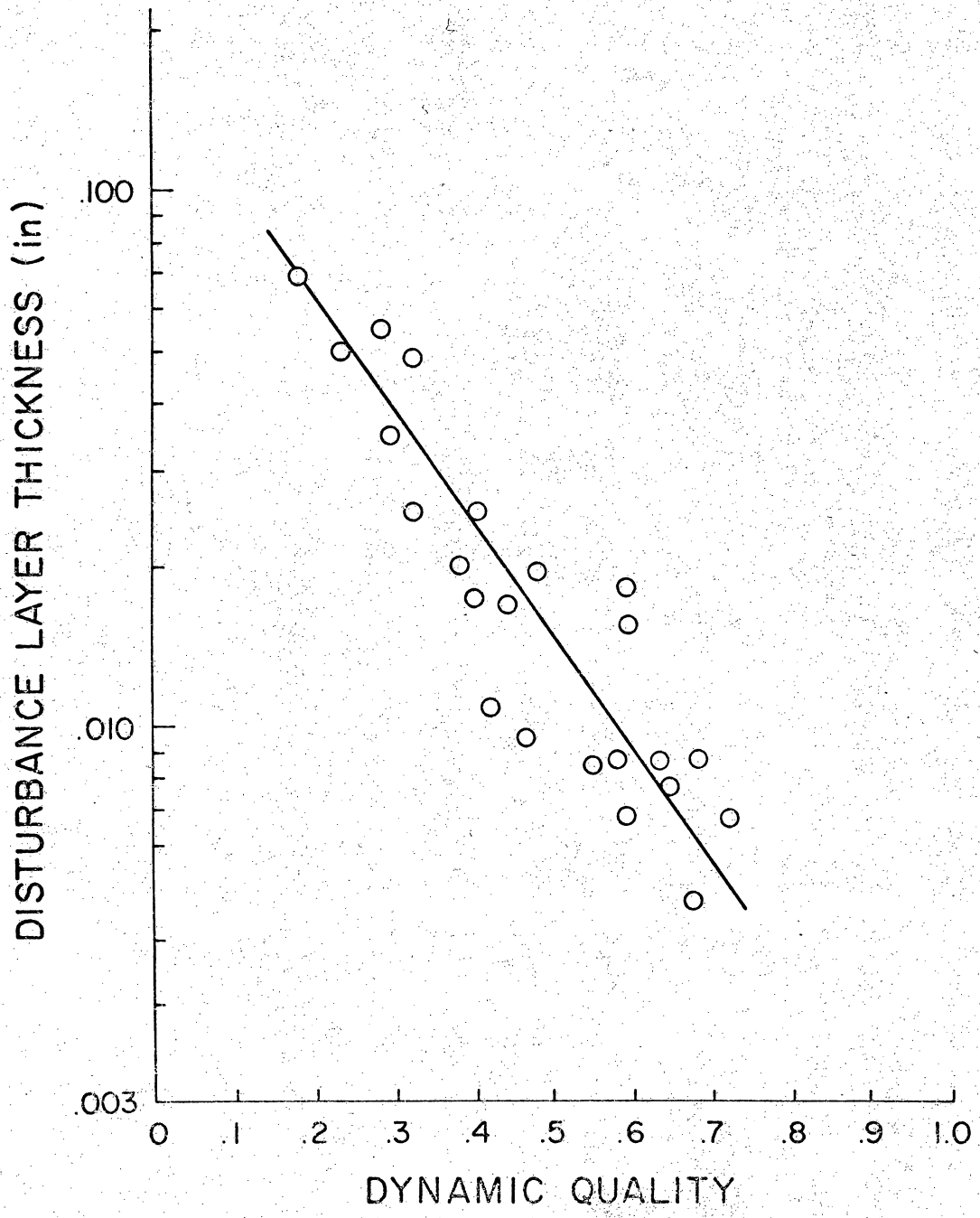

FIG. 17 THE DISTURBANCE LAYER THICKNESS AS A FUNCTION OF DYNAMIC QUALITY

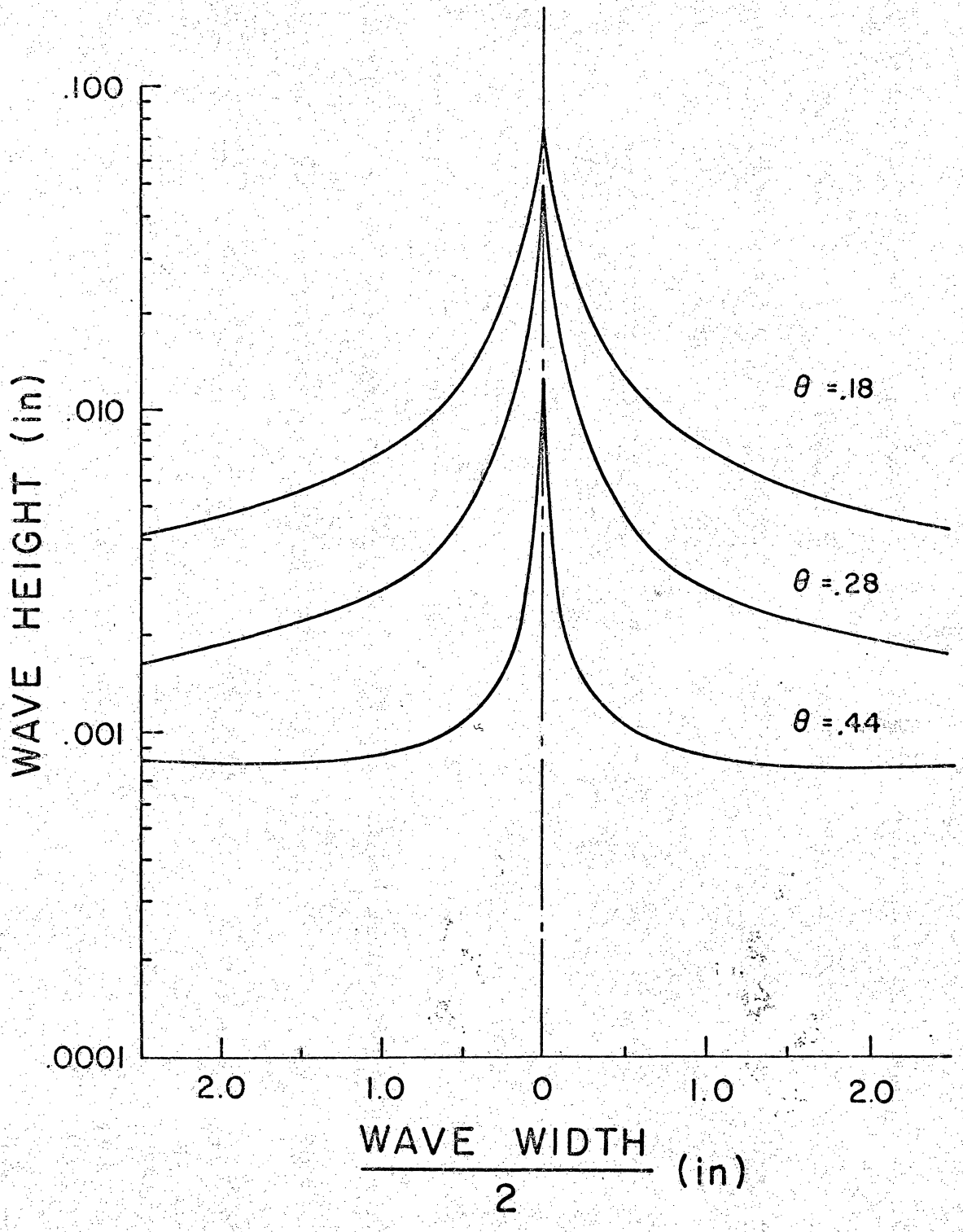

FIG. 18 STATISTICAL WAVE FORMS FOR SEVERAL DYNAMIC QUALITIES

equal amount of area under the curve of the statistical wave form represented this thickness. For the three typical statistical wave forms obtained, this film thickness agreed quite closely with the experimental mean film thickness.

Using the data for relative contact time and wave velocity, the liquid mass flow occurring in the waves was obtained by numerical integration over the disturbance layer. The result was the total amount of liquid which flows in the form of identifiable waves. For runs where the gas velocity was low, this total plus the liquid flow in the sublayer agreed closely with the liquid mass flow minus entrainment calculated from the axial energy balance. (The sublayer flow was determined by assuming a mean velocity equal to half the average wave velocity.) For runs with a high gas velocity, however, only about thirty percent of the difference between the total liquid mass flow and that accounted for by the entrainment correlation could be accounted for in the waves and in the sublayer. This result suggests the presence of much more entrainment in the form of spray or mist than the correlation given by Goss (15) predicts. This correlation, which was used in the axial energy balance, was obtained using an impact probe located at the center of a pipe in which there was a condensing annular-mist two phase flow. The resulting entrainment was assumed to be constant over the gaseous core. Since this correlation does not account for such a large portion of entrained

liquid, a radial entrainment gradient is concluded. Probably most of this liquid is a dense spray near the waves.

The percentage of the total liquid mass flow which occurs in the form of waves and in the continuous liquid sublayer was found to be a function of the gas velocity. This functional relationship is shown in Figure 19.

Most analyses of this type of flow involve the determination of the mean gas and liquid velocities. Usually, as in the present analysis, these are determined from an axial energy balance modified somewhat by an entrainment correlation. One of the results is a certain amount of liquid flowing with a certain velocity in an area defined by a characteristic film thickness. When the flow rate of liquid assumed to be in the film is too high, the result is an unreasonably high mean film velocity. Such is the case with the liquid velocities determined as described in Appendix B and listed in Table BII. A better approach would be either to assume the mean liquid velocity to be a certain fraction of the wave velocity, or to modify the entrainment correlation to include entrained liquid in the neighborhood of the waves.

As this discussion turns to some relationships involving the heat transfer, several results are noted. The heat transfer coefficients which are given in Table BI agreed rather well with those reported by Goodykoontz and Dorsch (9). Another result was that the film Nusselt number, based on the mean film thickness at the

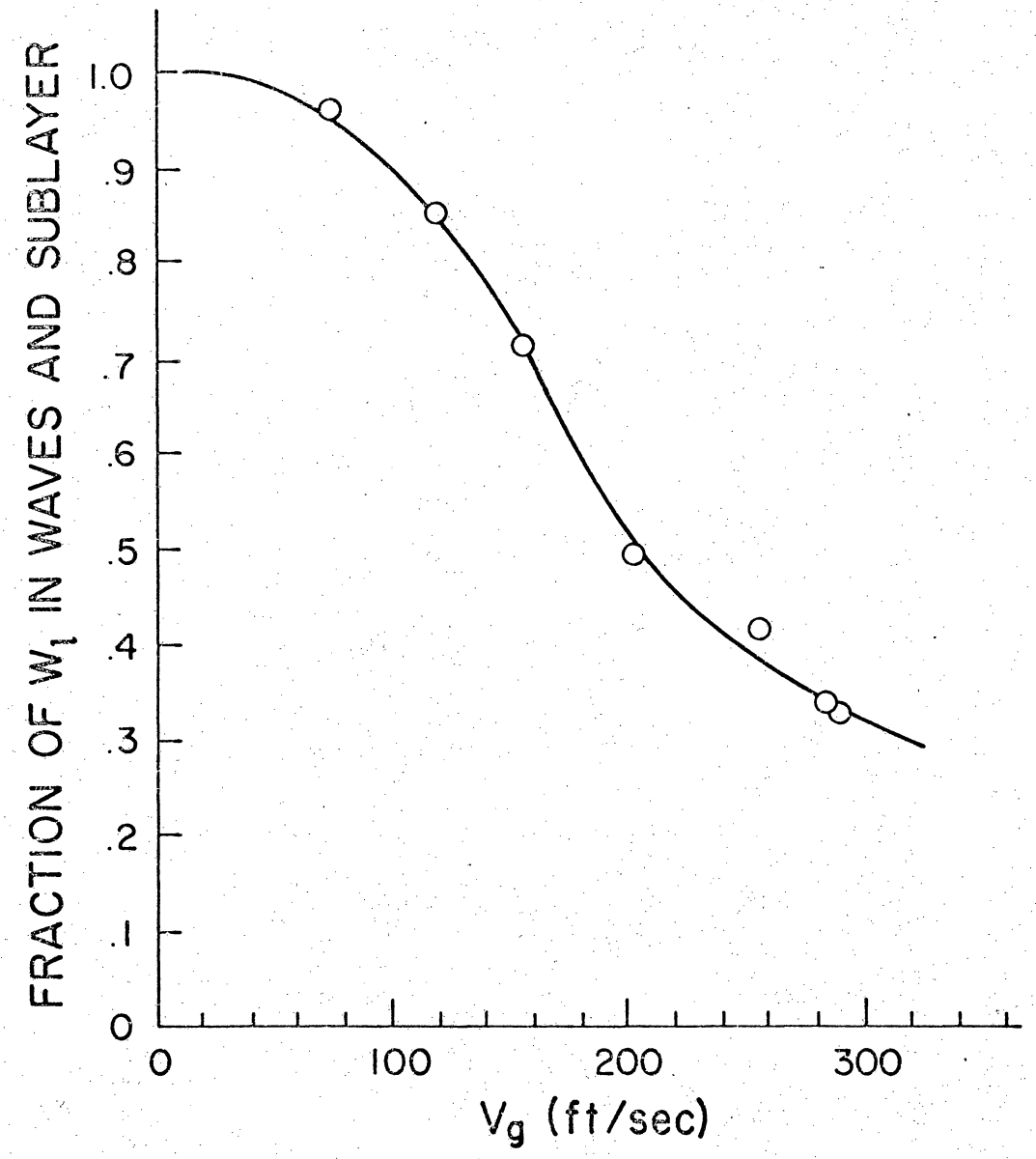

FIG. 19 FRACTION OF TOTAL LIQUID MASS FLOW OCCURING IN IDENTIFIABLE WAVES

location of the probes, was found to correlate roughly with the parameter $\theta(\rho_l/\rho_g)$. This correlation is shown in Figure 20. While the heat transfer coefficient increased with this parameter, an opposite trend for the film Nusselt ($Nu = h\delta/k_l$) was observed. This was because the film decreased at a faster rate than the heat transfer coefficient increased for increasing $\theta(\rho_l/\rho_g)$.

D. Experimental Error

Several factors in the experimental procedures and in the analysis give rise to some uncertainty in the results. The wall temperature measurements from the test section, which are given in Table CII, were somewhat scattered. This scatter, negligible for low water flow rates, was considerable at the higher cooling water flow rates. Much of this scatter is attributed to the entrance/exit effects which reduced the axisymmetry of the water flow. For counter flow conditions the cool water entering the condenser through a three-quarter inch pipe impinged directly on the one wall thermocouple located below the needle probe. This temperature was considerably lower than that measured just above the needle probes. For parallel flow conditions the scatter in the test section was less than for counter flow, but still significant for high water flows. This is attributed to the non-axisymmetric

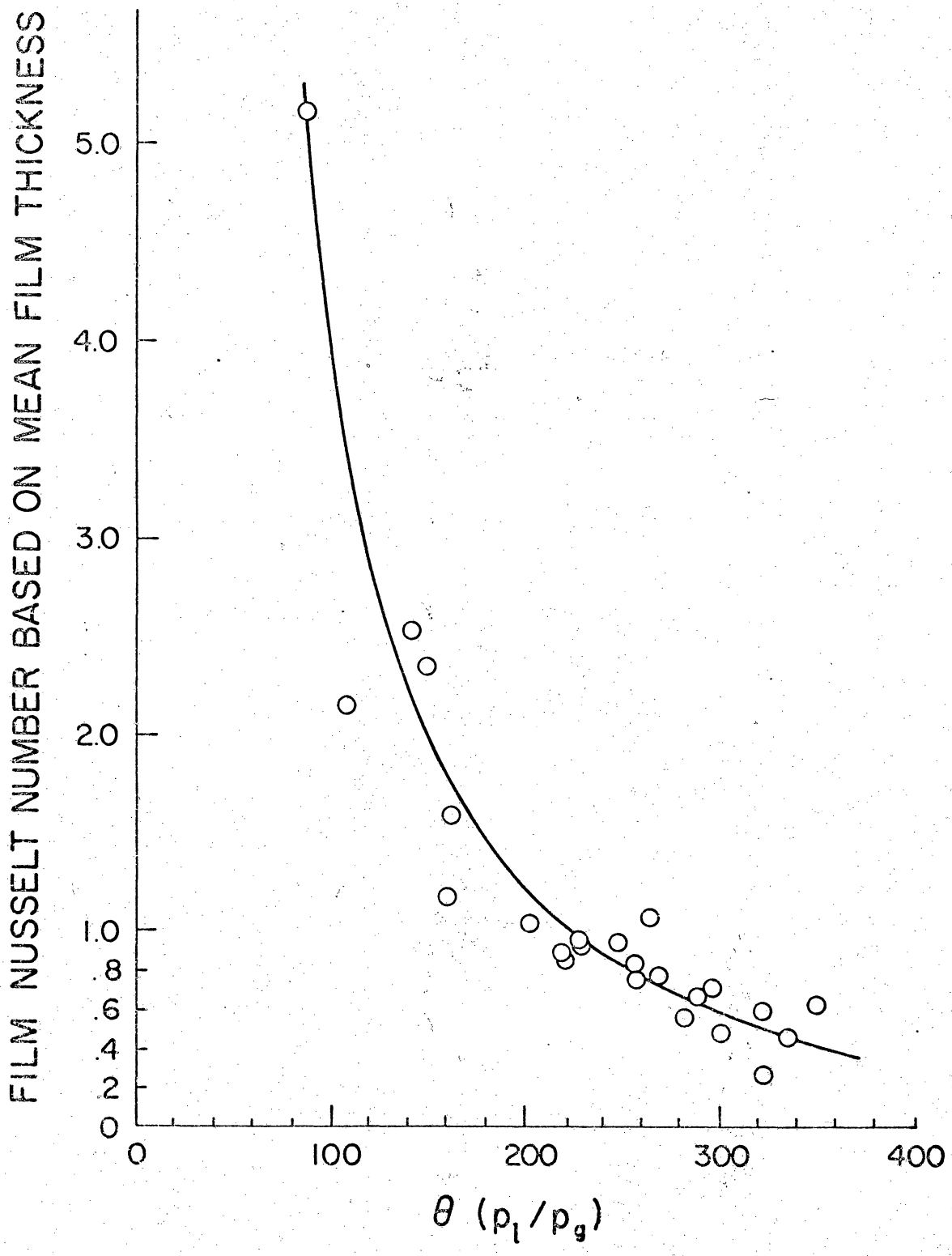

FIG. 20 LIQUID FILM NUSSELT NUMBER

flow pattern of the water leaving the test section. Of lesser importance, the rather low wall temperature at the top of the condenser for parallel flow conditions also resulted from impingement of cool water on the thermocouple. Another possible factor in the scatter of these data was the uneven surface conditions resulting from fouling.

The uncertainty which was of any importance lay in the determination of the wall temperature at the probes. In the analysis, the wall temperature was determined from the curve fit in which the lowest wall temperature measured in the test section and the highest on the condenser were weighted lightly.

As mentioned in a previous section, a blunt needle probe was tested. Better signal characteristics (less contact hysteresis) and a sharper termination of frequency as the probe neared the wall were the results. The probe with the pointed tip did not in all cases give a frequency which went to zero as the probe touched the continuous liquid sublayer. The contact area on the tip itself fluctuated as waves passed, even when the point was continuously submerged. The resulting voltage fluctuations continued to trigger the counter. Some uncertainty, therefore, arose in the determination of the liquid sublayer thickness. Both types of probes, however, gave identical results over most of the liquid layer.

VII. CONCLUSIONS

The film surface in a condensing flow appears to consist not only of distinct waves, but of a dense spray. The flow of this loose spray may amount to as much as seventy percent of the total liquid mass flow rate for high gas velocities.

The time averaged form of the waves has a long narrow peak; a form of wave which is rather short-lived. This indicates that the waves are constantly being formed and subsequently destroyed by the high speed gas.

The presence of spray in a condensing flow appears to be more prominent than for an air-water flow where the liquid and gas flow rates are constant over the flow length.

The local Nusselt number, based on the mean film thickness, correlated with the mass parameter $\theta(\rho_l/\rho_g)$.

Further investigation of the wave velocities with a blunt probe, or even an impact probe, would yield fruitful results. More accurate liquid mass flow rates could be determined for the liquid layer. In addition, an analytical model involving an experimentally determined density profile could be employed to give a more accurate prediction of two-phase flows of this type.

VIII. REFERENCES

1. Bell, K.J., J. Taborek, and F. Fenoglio, "Interpretation of Horizontal Intube Condensation Heat Transfer Correlations Using a Two-Phase Flow Regime Map," Eleventh National Heat Transfer Conference A.I.Ch.E-A.S.M.E., A.I.Ch.E. Preprint 18, 1969.

2. McManus, H.N., "An Experimental Investigation of Film Establishment, Film Profile Dimensions, and Surface Conditions in Two-Phase Annular Flow," Ph.D. Thesis, University of Minnesota, 1956.

3. Swanson, R.W., "Characteristics of the Gas-Liquid Interface in Two-Phase Annular Flow," Ph.D. Thesis, University of Delaware, 1964.

4. Lilleleht, L.U. and T.J. Hanratty, "Relation of Interfacial Shear Stress on the Wave Height for Concurrent Air-Water Flow," A.I.Ch.E. Journal, Vol. 7, No. 4, December, 1961, pp. 548-550.

5. Wallis, G.B., "Annular Two-Phase Flow - Part I: A Simple Theory," ASME Paper No. 69-FE-45.

6. Pletcher, R.H. and H.N. McManus, "Heat Transfer and Pressure Drop in Horizontal Annular Two-Phase, Two-Component Flow," International Journal of Heat and Mass Transfer, Vol. 11, July 1968, pp. 1087-1104.

7. Soliman, M., J.R. Schuster, and P.J. Berenson, "A General Heat Transfer Correlation for Annular Flow Condensation," Journal of Heat Transfer, Trans. ASME, Series C, Vol. 90, May 1968, pp. 267-276.

8. Dukler, A.E., M. Wicks, III, and R.G. Cleveland, "Frictional Pressure Drop in Two Phase Flow: A Comparison of Existing Correlations for Pressure Loss and Holdup," A.I.Ch.E. Journal, Vol. 10, No. 1, 1964, pp. 38-43.

9. Goodykoontz, J.H., and R.G. Dorsch, "Local Heat-Transfer Coefficients and Static Pressures for Condensation of High-Velocity Steam Within a Tube," NASA TN D-3953, May 1967.

10. Robson, F.L., and W.E. Hilding, "Final Report in the Study of Heat Transfer and the Flow Mechanics of Vapor Condensing in Small Straight Tubes: Part I. Experimental Measurements of the Wave Characteristics of Condensing Flow in a Horizontal Tube," NASA Project NsG-204-62S1, December 1965.

11. Collier, J.G., and G.F. Hewitt, "Film-Thickness Measurements," ASME Paper No. 64-WA/HT-41.

12. Bergles, A.E., "Electrical Probes for Study of Two-Phase Flows," Two-Phase Flow Instrumentation Volume, Eleventh National Heat Transfer Conference, Minneapolis, Minn., August, 1969.

13. Chien, S.F., and W. Ibele, "Pressure Drop and Liquid Film Thickness of Two-Phase Annular and Annular-Mist Flows," Journal of Heat Transfer, Trans. ASME, Series C, Vol. 86, 1964, pp. 89-86.

14. Zivi, S.M., "Estimation of Steady-State Steam Void-Fraction by Means of the Principle of Minimum Entropy Production," Journal of Heat Transfer, Trans. ASME, Series C, Vol. 86, No. 2, May 1964, pp. 247-252.

15. Goss, W.P., "Two-Phase, Annular-Mist Flow," Ph.D. Thesis, University of Connecticut, 1967.

16. System 360 Scientific Subrouting Package, (360A-CM-03X) Version III Programmer's Manual, International Business Machines Corporation, White Plains, New York, 1968.

17. Schied, F., Schaum's Outline of Theory and Problems of Numerical Analysis, McGraw-Hill Book Company, New York, N.Y., 1968.

18. Bruges, E.A., B. Latto, and A.K. Ray, "New Correlations and Tables of the Coefficient of Viscosity of Water and Steam Up to 1000 Bar and 1000 Deg. C," International Journal of Heat and Mass Transfer, Vol. 9, No. 5, May, 1966, pp. 465-480.

19. Keenan, J.H., and F.G. Keyes, Thermodynamic Properties of Steam, John Wiley and Sons, Inc., New York, N.Y., 1936.

IX. APPENDICES

Appendix A

Calculation of Polynomials for Least Squares Fit of Experimental Data

All of the calculations described below which involve fitting curves to the data were performed on an IBM 360, Model 50/65 digital computer. A library of scientific subroutines given in Reference (16) and available to the computer was employed several times in these calculations.

By using the method of least squares, a general polynomial was obtained which fit a given set of experimental data which consisted of argument and corresponding function values. This polynomial was formed from a series of Chebyshev polynomials and may be represented by

$$P(x) = \sum_{i=o}^{n} a_i T_i(x) \qquad \text{(A1)}$$

where $T_i(x)$ is a Chebyshev polynomial of the order i and n is the order of P(x). The first two polynomials are

$$T_0(x) = 1$$

$$T_1(x) = x \quad .$$

The successive polynomials can be obtained from the recursion formula,

$$T_i(x) = 2xT_{i-1}(x) - T_{i-2}(x) \quad .$$

These Chebyshev polynomials were ideal source functions for fitting experimental data because they possess the property of equal distribution of error. A more detailed discussion of the application of these polynomials is given in Reference (17).

For each run five sets of data were fitted with smooth curves. These sets are the static pressure, the wall temperature, and the cooling water temperature as a function of the axial position; wave frequency as a function of the common logarithm of the probe position; and the common logarithm of the probe position as a function of the relative contact time. For this last curve the relative contact time was used as the argument since the probe position at fifty percent relative contact time could be obtained directly from the curve fit. Using the logarithm of the probe position here gives a better graphic indication of the dependence of the wave frequency and relative contact time on the probe position. This practice is common in the literature (11), (12).

The computer subroutines APCH and APFS of Reference (16) were employed to calculate the values of a_i, (i = o,n). These coefficients for the different sets of data are listed in Tables AI through AV. The number of coefficients listed in the tables, (n+1), is the number of Chebyshev polynomials used to obtain P(x).

Since the use of Chebyshev polynomials for this purpose requires arguments in the range (-1, +1), all arguments in the input data were normalized in the above subroutines. Therefore, in

calculating the smoothed function values from P(x) for a certain set of data the following procedure was used. The input argument x' (i.e., L or $\log_{10}$h) was transformed by the relation

$$x = x' \, x_D + x_0 \tag{A2}$$

where x_D and x_0 are the normalization constants given also in Tables AI through AV. This value of x and the polynomial coefficients were then substituted into the expression for P(x) to give the desired function value.

The following is an example of the above calculation using the tables.

Example: Calculation of the cooling water temperature at L = 5.5 ft for Run 20.

From Table AI for Run 20

x_D = .177

x_0 = -1.00

a_0 = 85.57

a_1 = -19.09

a_2 = -1.68

Transforming L gives

$x = L \, x_D + x_0$

$= (5.5) \, (.177) - 1.00$

$= .0265$

Then,

$$P(x) = a_o T_o(x) + a_1 T_1(x) + a_2 T_2(x)$$

$$= 85.57 - 19.09x - 1.68(2x^2-1)$$

$$= 85.57 + .51 + 1.68$$

$$= 87.76 \text{ (F)}$$

Calculations such as this one were performed on the computer by subroutine CNPS of Reference (16).

TABLE AI

Coefficients of Chebyshev Polynomials and Normalization Constants

for Least Squares Fit of Cooling Water Temperature vs. Length

Run	a_0	a_1	a_2	x_D	x_0
13	79.02	-15.71	- .74	.177	-1.00
14	78.48	-15.30	- .82		
15	76.85	-15.30	- .71		
16	76.91	-15.84	- .95		
17	77.02	-16.51	-1.25		
18	79.40	-16.37	- .68		
19	87.18	-18.78	-1.54		
20	85.57	-19.09	-1.68		
21	84.85	-19.72	-1.61		
22	83.06	-18.51	-1.60		
23	99.26	-28.54	-1.42		
24	100.70	-28.52	-1.31		
25	100.93	-28.87	-1.39		
26	137.39	-59.24	-6.60		
27	127.95	-58.04	-5.59		
28	131.68	-58.60	-5.63		
29	79.51	-17.42	- .19		
30	79.84	-17.48	- .11		
31	80.37	-17.96	.15		
32	81.33	-18.48	- .06		
33	80.65	16.76	- .62		
34	99.05	29.93	- .82		
35	131.64	54.49	-5.71		
36	81.93	16.12	- .41		

TABLE AII

Coefficients of Chebyshev Polynomials and Normalization Constants

for Least Squares Fit of Wall Temperature vs. Length

Run	a_0	a_1	a_2	a_3	x_D	x_0
13	242.21	-17.92	-12.65	-3.59	.176	-1.00
14	237.72	-22.80	-16.68	-5.43		
15	236.69	-27.23	-17.80	-6.14		
16	243.40	-18.15	-12.68	-3.49		
17	242.78	-18.86	-12.32	-4.03		
18	243.43	-26.20	-17.78	-4.44		
19	257.42	-17.61	-10.32	- .72		
20	258.11	-17.16	-11.57	- .87		
21	260.32	-21.53	-12.18	-3.69		
22	250.52	-23.78	-15.99	-2.93		
23	269.60	-13.10	- 6.75	-1.10		
24	272.93	-12.16	- 6.05	- .99		
25	273.51	-12.36	- 6.60	- .82		
26	273.20	-10.31	- 2.34	- .64		
27	273.21	-10.29	- 2.33	- .18		
28	275.01	-10.62	- 2.87	- .79		
29	244.17	-17.13	-12.81	-2.52		
30	245.39	-18.06	-13.67	-2.54		
31	246.63	-18.66	-13.96	-3.13		
32	246.21	-21.44	-15.55	-4.67		
33	243.07	- 6.37	- 7.39	5.41		
34	268.26	- 5.44	- 2.77	2.36		
35	275.32	- 4.12	.20	.27		
36	242.71	- 5.99	- 9.44	6.23		

TABLE AIII

Coefficients of Chebyshev Polynomials and Normalization Constants

for Least Squares Fit of Pressure vs. Length

Run	a_0	a_1	a_2	a_3	x_D	x_0
13	44.54	-4.79	.820	.152	.176	-1.00
14	49.39	-2.05	.627	.894		
15	51.12	-1.34	.507	-.039		
16	45.67	-4.68	.747	.096		
17	45.13	-4.16	.674	.096		
18	49.97	-1.90	.515	.088		
19	47.65	-3.98	.316	.136		
20	48.89	-3.69	.326	.081		
21	53.21	-2.36	.324	.068		
22	49.77	-1.11	.200	.070		
23	52.79	-3.87	.196	.041		
24	57.44	-2.63	.201	.079		
25	58.67	-2.30	.167	.027		
26	54.30	-3.73	.097	.016		
27	54.98	-2.40	.123	.046		
28	58.64	-1.70	.051	.038		
29	46.71	-4.73	.867	.106		
30	49.10	-4.16	.843	.103		
31	51.17	-3.27	.740	.096		
32	54.28	-2.35	.700	.082		
33	45.64	-4.03	.746	.050		
34	53.88	-3.71	.260	.038		
35	53.33	-3.50	.160	-.011		
36	46.96	-3.68	.778	.077		

TABLE AIV

Coefficients of Chebyshev Polynomials and Normalization Constants

for Least Squares Fit of $Log_{10}h$ vs. Relative Contact Time

Run	a_0	a_1	a_2	a_3	x_D	x_0
13	-2.78	-.666	.146	-.115	.020	-1.00
14	-2.36	-.842	.041	-.033	.020	-1.00
15	-1.91	-.583	.075	-.069	.022	-1.07
16	-2.96	-.734	.102	-.138	.020	-1.04
17	-2.95	-.764	.055	-.137	.020	-1.04
18	-2.27	-.700	.081	-.131	.020	-1.00
19	-3.02	-.661	.134	-.164	.020	-1.00
20	-2.96	-.724	.120	-.087	.021	-1.11
21	-2.75	-.797	.076	-.123	.020	-1.00
22	-2.43	-.852	.043	-.187		
23	-3.09	-.621	.163	-.208		
24	-2.96	-.677	.133	-.224		
25	-2.83	-.738	.126	-.170		
26	-3.08	-.554	.193	-.164		
27	-3.12	-.702	.230	-.273		
28	-2.96	-.919	.070	-.201		
29	-2.82	-.772	.159	-.128		
30	-2.82	-.897	.079	-.094		
31	-2.73	-.909	.063	-.120		
32	-2.47	-.936	.018	-.132		
33	-2.83	-.822	.132	-.106		
34	-3.05	-.752	.072	-.104		
35	-3.29	-.608	.174	-.319		
36	-2.82	-.935	.128	-.133		

TABLE AV

Coefficients of Chebyshev Polynomials and Normalization Constants

for Least Squares Fit of Wave Contact Frequency vs. $\text{Log}_{10}h$

Run	a_0	a_1	a_2	a_3	a_4	a_5	a_6	x_D	x_0
13	67.10	30.33	-113.72	-15.50	52.12	-11.35	-	1.27	3.33
14	46.12	16.59	- 50.61	-16.42	7.61	.43	-	1.13	2.65
15	30.52	24.98	- 21.17	- 5.38	- 2.03	.97	-	1.53	2.76
16	68.90	19.35	- 67.49	-27.91	36.67	9.55	-29.78	.99	2.94
17	72.19	16.33	- 82.78	-20.80	28.18	7.20	- 8.87	.99	2.95
18	44.34	1.29	- 52.54	- .98	9.61	- .50	3.10	1.17	2.51
19	107.93	17.94	-131.31	-33.52	63.13	16.98	-32.01	1.02	3.09
20	88.86	18.31	-102.75	-35.04	50.44	11.72	-32.41	1.02	3.06
21	87.68	4.50	- 96.40	- 9.68	29.27	11.41	- 6.74	1.02	2.76
22	52.54	1.67	- 38.84	-20.60	3.24	13.68	- 7.17	.84	2.11
23	68.59	3.65	-103.19	.23	60.93	- 9.88	-25.89	1.03	3.14
24	82.39	- 1.90	- 96.25	-12.60	51.81	8.05	-30.22	.94	2.74
25	81.90	- 2.04	-100.94	.36	42.07	-10.44	-14.56	1.04	2.84
26	84.79	-42.94	- 97.09	52.38	17.64	-30.49	18.26	1.31	3.83
27	119.91	-55.99	- 98.91	30.97	47.07	-26.02	- 9.20	.94	2.78
28	144.17	-41.34	-134.09	- .58	69.82	-42.73	15.45	.89	2.54
29	72.06	-47.50	- 52.35	17.98	18.51	- 9.08	2.00	1.01	2.73
30	83.48	-37.52	- 61.89	- 3.08	19.98	.50	.93	.86	2.50
31	93.52	-40.17	- 67.56	- .26	17.51	- 1.26	2.81	.96	2.56
32	66.96	- 6.89	- 71.58	- 6.63	19.82	.60	1.65	.93	2.27
33	77.68	-49.83	- 47.19	11.56	11.96	- 3.12	1.14	1.02	2.79
34	42.20	-26.38	- 25.56	9.55	3.96	- .64	- 1.87	1.07	3.27
35	23.67	- .22	- 43.58	3.78	30.68	-25.54	12.24	1.05	3.20
36	88.76	-39.31	- 67.43	- 4.84	27.00	- 3.69	1.07	.84	2.35

Appendix B

Reduction of Experimental Data

The local heat flux based on the inside area of the pipe is calculated from a radial energy balance

$$q = \frac{W_{cw}\, c_{p,cw}}{\pi D_i} \frac{dT_{cw}}{dL} , \tag{B1}$$

where $c_{p,cw}$ is the specific heat for water at 100 F and 14.7 psia. The term dT_{cw}/dL represents the slope of the curve that was fit to the experimental data for T_{cw} as a function of L. Discrete points taken at regular argument intervals from this smooth curve were transferred to the subroutine DGT3 (16) which calculated the slope using an interpolating polynomial.

The local heat transfer coefficient is defined as

$$h_{cl} \equiv \frac{q}{T_g - T_{iw}} \tag{B2}$$

The inside wall temperature, T_{iw}, in (B2) is obtained from the equation for radial heat conduction through the tube wall,

$$T_{iw} = T_{ow} + \frac{qD_i \ln(D_o/D_i)}{2\, k_{cu}} \tag{B3}$$

The value of k_{cu} is 217 (B/hr-ft-F), which is the thermal conductivity of copper at 280 F. This is a characteristic temperature of the copper pipe for the data taken.

The rate of total heat removed from the steam between the entrance and the needle probes is

$$Q_t = W_{cw}\, c_{p,cw}\, \Delta T_{cw} \tag{B4}$$

where ΔT_{cw} is the temperature drop of the cooling water between these two locations.

The mean and the modal film thicknesses were each used to calculate the gas and liquid flow areas. These are given as

$$A_g = \pi(D_i - 2\delta)^2/576 \tag{B5}$$

$$A_l = \pi\delta(D_i - \delta)/144 \tag{B6}$$

where δ represents the respective value of film thickness used.

In the calculation of mean gas and liquid velocities the following axial energy balance was employed.

$$\frac{Q_t}{W_t} - H_o + \frac{W_l}{W_t}\left[H_l + \frac{V_l^2}{2g_cJ}\right] + \theta\left[H_g + \frac{V_g^2}{2g_cJ}\right] + \frac{W_e}{W_t}\left[H_l + \frac{(.9\ V_g)^2}{2g_cJ}\right] = 0 \tag{B7}$$

Equation (B7) assumes that the entrained particles move with a velocity that is ninety percent of the gas velocity. The entrainment flow rate, W_e, in (B7) is calculated from an entrainment correlation given by Goss (15) which is expressed in parametric form as

$$\theta = K\left[(1 - b_1)s - b_2 s^2 - b_3 s^3 - b_4 s^4 \right] \qquad \text{(B8a)}$$

$$\chi = 2Ks - \theta \qquad \text{(B8b)}$$

where

$K = .707107$

$b_1 = .638377$

$b_2 = 1.137108$

$b_3 = -2.246491$

$b_4 = .794254$

These equations (B7) and (B8) were solved iteratively by the following process.

1. θ was initialized at a low value, .10.
2. Using this value of θ, Eq. (B8a) was solved for s. Since $0 < s < \sqrt{2}$, a unique solution existed.
3. χ was obtained from Eq. (B8b) using the values of θ and s from steps 1 and 2.
4. The following calculations were then performed to obtain local flow rates and velocities.

$$W_g = \theta W_t$$

$$W_e = W_g/\chi - W_g$$

$$W_l = W_t - W_g - W_e$$

$$V_l = W_l/\rho_l A_l$$

$$V_g = W_g/\rho_g A_g$$

5. At this point all quantities in Eq. (B7) had been determined. These values were then substituted into (B7). If the expression on the left of the equal sign was negative, θ was increased by .1 and the above steps were repeated. This process was continued until the expression in (B7) became positive, at which time θ was decreased successively by .01 until a sign change in the expression occurred again. As before, θ was then increased, but this time by .001 and when the sign of the expression in (B7) changed a fourth time the procedure stopped. The most recent values calculated in step 4 and the most recent value of θ (to the nearest .001) were taken as the solution.

The remaining parameters calculated were the following.

1. The gas Reynolds number

$$R_{e_g} = \frac{\rho_g V_g (D-2\delta)}{12\ \mu_g} \tag{B9}$$

2. The liquid Reynolds number

$$R_{e_l} = \frac{\rho_l V_l \delta}{12\ \mu_l} \tag{B10}$$

3. The superficial gas Reynolds number

$$R'_{e_g} = \frac{4W_g}{\pi D_i \mu_g} \tag{B11}$$

4. The superficial liquid Reynolds number

$$R'_{e1} = \frac{4W_1}{\pi D_i \mu_1} \tag{B12}$$

5. The film Nusselt number

$$Nu = \frac{h\delta}{k_1} \tag{B13}$$

It should be noted that δ represents in Eqs. (B9), (B10), and (B13) the film thickness used, modal or mean. The viscosities were obtained from a correlation given by Bruges, Latto, and Ray (18). The densities and the thermal conductivity of the water in the liquid film were taken from Reference (19).

TABLE BI

Heat Transfer Results

L (ft)	Run 13 $q \times 10^{-3}$ (B/hr-ft^2)	Run 13 h_c (B/hr-ft^2-F)	Run 13 ΔT_f (F)	Run 14 $q \times 10^{-3}$ (B/hr-ft^2)	Run 14 h_c (B/hr-ft^2-F)	Run 14 ΔT_f (F)
0	138.4	5640	24	127.5	4470	29
1	140.4	6390	22	133.6	4830	28
2	145.9	7570	19	139.7	5460	22
3	151.5	9270	16	145.8	6360	23
4	157.0	11460	14	151.9	7420	20
5	162.6	13740	12	158.0	8370	19
6	168.1	14940	11	164.1	8680	19
7	173.7	13940	12	170.2	8000	22
8	179.2	11220	16	176.3	6610	27
9	184.8	8280	22	182.4	5090	35
10	190.3	5960	32	188.5	3810	49
11.05	196.2	4240	46	194.9	2810	69
	Run 15			Run 16		
0	133.6	5060	27	121.0	4970	24
1	138.9	5200	27	127.7	5720	23
2	144.2	5660	25	134.4	6850	19
3	149.6	6350	24	141.2	8420	17
4	154.9	7150	21	147.9	10400	15
5	160.3	7750	21	154.6	12380	12
6	165.6	7770	22	161.4	13390	12
7	170.9	7000	24	168.1	12560	13
8	176.3	5730	30	174.8	10300	17
9	181.6	4410	44	181.5	7220	23
10	187.0	3310	56	188.3	5720	32
11.05	192.6	2450	78	198.4	4168	47

TABLE BI (continued)

Heat Transfer Results

L (ft)	Run 17 $q \times 10^{-3}$ (B/hr-ft^2)	Run 17 h_c (B/hr-ft^2-F)	Run 17 ΔT_f (F)	Run 18 $q \times 10^{-3}$ (B/hr-ft^2)	Run 18 h_c (B/hr-ft^2-F)	Run 18 ΔT_f (F)
0	111.4	4830	23	132.4	5940	22
1	120.0	5510	22	137.1	6820	20
2	128.6	6570	19	141.8	8140	17
3	137.2	8090	17	146.5	9890	15
4	145.8	10050	15	151.2	11760	13
5	154.4	12120	12	155.8	12790	13
6	163.0	13340	12	160.5	12000	13
7	171.6	12720	13	165.2	9700	17
8	180.1	10530	17	169.9	7160	23
9	188.7	8000	24	175.6	5121	35
10	197.3	5880	33	179.2	3680	49
11.05	206.3	4270	48	184.1	2660	69
	Run 19			Run 20		
0	70.9	4710	15	70.0	3880	17
1	77.1	6840	11	73.4	5750	13
2	83.2	10110	8	79.8	8750	10
3	89.3	14660	6	86.2	13290	7
4	95.5	19290	5	92.6	18610	5
5	101.6	20630	5	99.8	20940	5
6	107.8	17580	6	105.4	18000	6
7	113.9	13100	8	111.9	13140	8
8	120.0	9440	12	118.3	9240	13
9	126.2	6880	19	124.7	6610	19
10	132.3	5150	26	131.1	4880	27
11.05	138.8	3920	35	137.8	3690	37

TABLE BI (continued)

Heat Transfer Results

L (ft)	Run 21 $q \times 10^{-3}$ (B/hr-ft^2)	Run 21 h_c (B/hr-ft^2-F)	Run 21 ΔT_f (F)	Run 22 $q \times 10^{-3}$ (B/hr-ft^2)	Run 22 h_c (B/hr-ft^2-F)	Run 22 ΔT_f (F)
0	71.9	6090	12	65.5	3550	18
1	78.0	6810	11	71.6	4630	15
2	84.2	8130	11	77.7	6160	13
3	90.3	10040	9	83.8	8120	10
4	96.5	12300	8	90.0	10020	9
5	102.6	13840	7	96.1	10710	9
6	108.7	13260	8	102.2	9550	10
7	114.9	10750	11	108.3	7440	14
8	121.0	7880	15	114.4	5460	21
9	127.1	5590	23	120.6	3990	31
10	133.3	4000	32	126.7	2960	43
11.05	139.7	2890	57	133.1	2210	60
	Run 23			Run 24		
0	61.8	6400	10	62.5	6290	10
1	64.5	8050	8	65.0	7330	8
2	67.3	10310	6	67.5	8530	8
3	70.0	13140	6	70.0	9730	7
4	72.7	15850	5	72.5	10550	7
5	75.4	16980	5	74.9	10580	7
6	78.1	15460	5	77.4	9720	8
7	80.8	12320	6	79.9	8270	10
8	83.5	9160	9	82.4	6680	12
9	86.3	6690	13	84.9	5280	16
10	89.0	4940	18	87.4	4140	22
11.05	91.8	3670	25	90.0	3230	28

TABLE BI (continued)

Heat Transfer Results

L (ft)	Run 25 $q \times 10^{-3}$ (B/hr-ft^2)	Run 25 h_c (B/hr-ft^2-F)	Run 25 ΔT_f (F)	Run 26 $q \times 10^{-3}$ (B/hr-ft^2)	Run 26 h_c (B/hr-ft^2-F)	Run 26 ΔT_f (F)
0	62.6	5530	11	36.0	4880	8
1	65.3	6770	9	41.0	5480	8
2	67.9	8200	8	46.2	6160	7
3	70.6	9590	7	51.2	6843	7
4	73.2	10500	7	56.3	7480	7
5	75.9	10500	7	61.4	7940	8
6	78.5	9520	8	66.5	8140	8
7	81.2	8010	10	71.6	8020	9
8	83.8	6440	13	76.7	7601	10
9	86.5	5090	17	81.8	6960	12
10	89.1	4020	22	86.9	6210	14
11.05	91.9	3170	29	92.3	5401	17
	Run 27			Run 28		
0	41.5	6040	7	41.8	5320	8
1	46.1	6850	6	46.4	5550	9
2	50.7	7520	7	51.0	5840	8
3	55.3	7960	7	55.6	6140	9
4	59.9	8120	8	60.2	6380	10
5	64.4	8020	8	64.8	6480	10
6	69.0	7680	9	69.4	6400	11
7	73.6	7180	10	74.0	6120	12
8	78.2	6590	12	78.6	5680	13
9	82.8	5980	14	83.2	5140	16
10	87.4	5380	16	87.8	4560	20
11.05	92.2	4800	20	92.7	3960	23

TABLE BI (continued)

Heat Transfer Results

L (ft)	Run 29 $q \times 10^{-3}$ (B/hr-ft^2)	Run 29 h_c (B/hr-ft^2-F)	Run 29 ΔT_f (F)	Run 30 $q \times 10^{-3}$ (B/hr-ft^2)	Run 30 h_c (B/hr-ft^2-F)	Run 30 ΔT_f (F)
0	180.5	7060	26	185.0	7050	26
1	182.0	8320	22	185.8	8300	23
2	183.5	10060	19	186.7	9990	18
3	185.0	12320	15	187.5	12100	16
4	186.5	14870	13	188.3	14310	13
5	188.0	16800	11	189.1	15690	13
6	189.5	16780	11	189.9	15190	12
7	191.0	14400	13	190.7	12820	15
8	192.5	11110	17	191.5	9800	20
9	193.9	8090	24	192.3	7170	27
10	195.4	5840	34	193.1	5210	37
11.05	197.0	4190	48	193.9	3770	52
	Run 31			Run 32		
0	201.3	8140	25	198.0	7920	25
1	200.1	9150	22	198.4	8380	24
2	199.0	10560	19	198.9	9260	22
3	197.8	12310	16	199.3	10510	19
4	196.7	14070	14	199.7	11900	16
5	195.6	15030	13	200.2	12840	16
6	194.4	14330	13	200.6	12550	16
7	193.3	12010	16	201.0	10820	19
8	192.1	9140	21	201.5	8380	24
9	191.0	6640	29	201.9	6130	33
10	189.9	4780	39	202.3	4400	46
11.05	188.7	3414	55	202.8	3140	64

TABLE BI (continued)

Heat Transfer Results

L (ft)	Run 33 $q \times 10^{-3}$ (B/hr-ft^2)	Run 33 h_c (B/hr-ft^2-F)	Run 33 ΔT_f (F)	Run 34 $q \times 10^{-3}$ (B/hr-ft^2)	Run 34 h_c (B/hr-ft^2-F)	Run 34 ΔT_f (F)
0	213.8	3390	54	115.4	4380	26
1	208.9	5020	42	113.4	5240	21
2	204.1	6020	34	111.4	5942	19
3	199.2	6680	29	109.4	6310	17
4	194.4	6790	28	107.3	6280	17
5	189.5	6390	30	105.3	5940	18
6	184.7	5740	32	103.3	5450	19
7	179.8	5060	35	101.3	4950	20
8	175.0	4490	39	99.3	4520	22
9	170.1	4060	42	97.2	4200	23
10	165.3	3800	43	95.2	4020	25
11.05	160.2	3710	43	93.1	4000	23
	Run 35			Run 36		
0	107.2	6500	17	197.4	3420	58
1	101.6	6360	16	194.2	4460	43
2	96.0	6140	16	191.0	5560	34
3	90.4	5870	15	187.8	6380	30
4	84.9	5560	15	184.6	6610	28
5	79.3	5220	15	181.4	6240	29
6	73.7	4870	15	178.2	5550	32
7	68.1	4530	15	175.0	4850	36
8	62.5	4200	15	171.8	4250	40
9	56.9	3880	15	168.6	3820	44
10	51.3	3590	14	165.3	3550	47
11.05	45.4	3310	14	162.0	3470	47

TABLE BII

Summary of Flow Parameters

Run	W_{cw} (lbm/hr)	W_t (lbm/hr)	W_g (lbm/hr)	W_l (lbm/hr)	θ	$R'_{e_g} \times 10^{-3}$	$R'_{e_l} \times 10^{-3}$
13	11430	682	301	357	.44	191.5	14.46
14	11430	530	154	352	.29	96.7	14.91
15	11560	468	86	358	.18	53.8	15.33
16	10470	673	308	342	.46	195.7	13.93
17	10470	638	272	343	.42	172.7	13.99
18	10480	515	145	346	.28	90.9	14.71
19	6080	185	342	226	.58	216.2	9.33
20	5840	531	294	221	.55	185.0	9.25
21	5840	476	229	232	.48	142.4	9.99
22	5840	343	111	218	.32	69.3	9.26
23	2920	548	370	164	.67	231.5	6.99
24	2900	484	305	165	.63	188.9	7.27
25	2900	447	266	168	.59	163.9	7.46
26	1180	530	381	136	.72	237.7	5.84
27	1160	430	274	144	.64	170.4	6.27
28	1250	387	228	147	.59	140.9	6.52
29	11710	723	287	409	.40	181.8	16.79
30	11710	706	266	412	.38	167.6	17.24
31	11710	667	213	426	.32	133.2	18.10
32	11710	610	140	440	.23	87.2	19.10
33	12000	702	269	405	.38	170.9	16.59
34	3750	594	351	226	.59	219.0	9.69
35	1500	550	372	163	.68	231.8	7.06
36	12000	692	276	390	.40	174.5	16.13

TABLE BII (continued)

Summary of Flow Parameters

Run	V_g* (ft/sec)	V_g** (ft/sec)	V_l* (ft/sec)	V_l** (ft/sec)
13	283	285	88.0	41.6
14	126	129	26.4	14.7
15	70	75	10.7	4.8
16	282	282	114.4	79.3
17	250	250	99.3	79.7
18	118	119	23.0	14.5
19	297	298	95.0	58.8
20	248	248	73.8	57.8
21	174	174	45.6	34.2
22	89	90	19.2	11.4
23	290	291	85.1	54.0
24	216	216	60.8	38.7
25	183	184	44.8	28.0
26	290	290	75.0	63.2
27	201	202	79.0	53.4
28	156	156	46.4	48.6
29	157	157	114.5	106.5
30	224	224	95.7	96.0
31	170	170	78.4	70.3
32	105	105	40.4	36.6
33	244	244	107.6	105.5
34	270	268	87.2	132.3
35	277	277	106.3	85.3
36	241	241	102.4	90.7

* - Calculated using mean film thickness

** - Calculated using modal film thickness

TABLE BII (continued)

Summary of Flow Parameters

Run	Re_g* x 10^{-3}	Re_g** x 10^{-3}	Re_l* x 10^{-3}	Re_l** x 10^{-3}
13	192.4	193.4	3.62	3.63
14	98.3	99.5	3.75	3.76
15	56.0	59.0	3.88	3.95
16	196.3	196.6	3.49	3.49
17	173.4	173.6	3.50	3.50
18	92.5	93.5	3.70	3.71
19	216.8	217.1	2.34	2.34
20	185.6	185.8	2.32	2.32
21	143.3	143.6	2.50	2.50
22	70.2	70.9	2.33	2.33
23	232.1	232.4	1.75	1.75
24	189.6	189.9	1.82	1.82
25	164.7	165.1	1.87	1.87
26	238.2	238.2	1.46	1.46
27	170.7	170.9	1.57	1.57
28	141.5	141.4	1.63	1.63
29	182.6	182.6	4.20	4.20
30	168.4	168.4	4.32	4.32
31	134.0	134.1	4.53	4.53
32	88.3	88.4	4.79	4.80
33	171.7	171.7	4.15	4.15
34	219.7	219.5	2.43	2.42
35	232.2	232.4	1.77	1.77
36	175.2	175.3	4.04	4.04

* - Calculated using mean film thickness

** - Calculated using modal film thickness

TABLE BIII

Summary of Heat Transfer Parameters

Run	$h_c \times 10^{-3}$ (B/hr-ft^2-F)	$Q_t \times 10^{-3}$ (B/hr)	Nu*	Nu**	$\theta(\rho_l/\rho_g)$
13	4.19	358.9	1.06	2.25	265
14	2.78	349.5	2.34	4.20	149
15	2.42	353.6	5.15	11.58	88
16	4.10	343.0	.76	1.10	269
17	4.27	344.5	.92	1.15	247
18	2.66	343.3	2.52	4.02	142
19	3.92	227.3	.58	.94	322
20	3.68	222.1	.69	.88	296
21	2.89	229.5	.92	1.23	231
22	2.21	215.3	1.58	2.66	162
23	3.67	166.6	.44	.70	335
24	3.23	165.3	.55	.87	282
25	3.17	167.6	.75	1.20	258
26	5.40	139.0	.61	.73	349
27	4.80	145.0	.46	.81	300
28	3.96	145.8	.79	.75	256
29	4.19	409.4	.94	1.01	228
30	3.77	410.9	1.02	1.01	203
31	3.41	422.9	1.16	1.30	161
32	3.14	434.6	2.15	2.38	108
33	3.71	405.5	.87	.89	220
34	4.00	226.1	.65	.43	288
35	3.30	165.5	.24	.40	322
36	3.47	389.7	.83	.93	222

* - Calculated using mean film thickness

** - Calculated using modal film thickness

TABLE BIV

Summary of Film Parameters

Run	$\delta_m \times 10^3$ (in)	$\delta_{md} \times 10^3$ (in)	$\delta_s \times 10^3$ (in)	$\delta' \times 10^3$ (in)	$\frac{(\delta_m - \delta_s)}{\delta'} \times 10^3$
13	1.18	2.51	.8	16.98	22.7
14	3.93	7.08	.8	34.68	90.4
15	9.96	22.39	2.0	68.80	115.6
16	.87	1.26	.4	9.55	44.2
17	1.01	1.26	.3	10.92	65.0
18	4.43	7.08	1.3	54.93	57.0
19	.69	1.12	.3	8.61	45.8
20	.88	1.12	.4	8.51	56.3
21	1.50	1.99	.4	19.55	56.1
22	3.33	5.62	.7	49.42	53.2
23	.56	.89	.3	4.71	56.3
24	.80	1.26	.3	8.61	58.2
25	1.11	1.78	.4	15.45	46.0
26	.53	.63	.3	6.78	34.2
27	.53	.79	.2	7.74	32.3
28	.93	.89	.3	18.00	32.2
29	1.05	1.12	.4	17.38	37.2
30	1.26	1.26	.3	19.65	49.0
31	1.60	1.78	.3	24.82	52.2
32	3.21	3.55	.5	49.62	54.7
33	1.10	1.12	.3	19.65	40.7
34	.76	.50	.3	6.78	67.9
35	.45	.56	.2	8.71	16.2
36	1.11	1.26	.3	24.82	32.8

Appendix C

Experimental Data

TABLE CI

Measured Cooling Water Temperatures (F)

L (ft)	Run 13	14	15	16	17	18	19	20
0	94	94	92	92	93	95	104	104
.39	91	91	90	90	91	93	103	101
.81	95	91	89	89	90	93	102	101
1.23	91	90	88	89	90	92	102	100
1.64	91	90	88	89	89	92	101	100
2.06	89	89	87	89	88	91	100	98
2.47	87	87	86	86	87	89	99	97
2.89	88	87	86	86	86	89	98	96
3.31	87	87	85	86	86	88	98	96
3.73	83	82	81	81	82	84	93	91
4.14	83	82	81	81	82	84	93	92
4.56	83	82	80	82	81	84	93	91
4.97	80	80	79	78	78	80	89	87
5.39	80	80	78	77	78	79	88	88
5.81	79	79	77	77	78	79	87	87
6.23	80	79	77	77	78	79	88	87
6.64	79	79	77	77	77	78	87	87
7.06	78	77	76	77	77	77	86	84
7.48	72	72	71	70	71	73	80	78
7.90	73	72	70	70	71	73	80	78
8.32	72	72	69	70	70	73	80	77
8.73	72	72	69	69	69	72	79	77
9.14	70	69	67	68	68	71	76	75
9.73	66	66	64	64	64	67	72	70
10.22	66	66	65	64	64	66	72	70
10.51	65	65	64	64	61	65	71	69
10.81	65	64	63	62	61	64	70	68
11.07	64	64	62	61	60	63	68	66
11.33	62	62	61	60	60	62	66	64

TABLE CI (continued)

Measured Cooling Water Temperatures (F)

L (ft)	Run 21	22	23	24	25	26	27	28
0	104	101	131	130	132	193	184	189
.39	101	97	122	124	125	186	176	179
.81	101	98	121	124	124	185	173	178
1.23	99	97	120	123	123	182	170	175
1.64	100	97	121	122	122	181	170	175
2.06	98	96	117	118	119	175	165	169
2.47	96	93	115	117	116	172	161	165
2.89	96	94	115	116	116	169	159	162
3.31	96	94	114	116	115	167	157	161
3.73	91	91	109	110	110	161	152	155
4.14	91	89	108	110	110	160	151	154
4.56	91	89	107	107	109	157	147	150
4.97	87	84	102	104	106	150	141	144
5.39	85	83	100	102	101	146	137	141
5.81	85	83	100	101	101	141	131	135
6.23	86	84	99	100	101	138	127	133
6.64	85	84	98	98	99	134	125	128
7.06	84	82	96	96	97	129	122	124
7.48	77	75	88	91	91	122	114	116
7.90	78	76	88	89	90	118	107	113
8.32	77	76	87	87	88	113	103	106
8.73	77	75	86	86	87	107	97	102
9.14	74	73	82	84	83	107	91	97
9.73	68	68	78	80	81	97	81	84
10.22	69	69	78	80	79	91	79	85
10.51	67	66	74	76	76	85	76	77
10.81	66	65	73	75	73	78	73	75
11.07	64	64	70	71	72	77	71	73
11.33	64	63	68	69	69	65	66	69

TABLE CI (continued)

Measured Cooling Water Temperatures (F)

L (ft)	Run 29	30	31	32	33	34	35	36
0	97	97	97	98	62	67	72	65
.39	96	97	97	98	64	71	80	65
.81	95	96	96	97	66	74	82	68
1.23	93	94	96	97	69	76	87	70
1.64	91	93	95	97	69	78	92	70
2.06	91	88	93	95	71	80	96	73
2.47	89	89	90	91	71	82	104	73
2.89	88	89	89	91	73	83	108	75
3.31	88	88	88	90	74	88	114	77
3.73	84	84	84	85	76	91	118	78
4.14	84	84	84	85	77	95	123	78
4.56	84	84	84	85	78	95	126	79
4.97	80	80	81	82	77	94	128	77
5.39	79	80	80	81	80	96	135	80
5.81	79	79	79	81	81	97	139	82
6.23	79	80	79	81	85	101	143	85
6.64	79	80	79	80	87	106	147	88
7.06	77	78	78	78	86	107	151	87
7.48	72	72	73	73	86	112	152	88
7.90	72	72	72	73	88	112	158	88
8.32	72	72	73	73	88	115	160	89
8.73	72	72	72	73	88	116	162	89
9.14	70	70	70	71	89	118	169	91
9.73	66	65	66	68	95	123	175	95
10.22	65	66	67	66	91	117	168	91
10.51	64	66	65	65	95	126	175	96
10.81	64	64	64	65	97	126	178	98
11.07	63	63	63	64	97	127	180	98
11.33	61	61	62	62	97	128	180	98

TABLE CII

Measured Wall Temperatures (F)

L (ft)	Run 13	14	15	16	17	18
.01	230	226	228	229	228	232
.81	257	255	257	259	260	264
1.64	247	244	245	247	247	251
2.47	255	254	256	257	255	262
3.31	250	248	250	251	251	256
4.14	254	252	254	254	254	260
4.97	243	241	242	244	243	250
5.81	251	250	246	253	251	258
6.64	247	247	247	249	249	253
7.48	250	249	250	251	251	254
8.32	249	247	246	250	249	249
9.14	217	207	201	217	221	216
9.73	225	214	206	227	228	222
10.30	223	215	209	222	221	219
10.63	227	214	206	228	226	219
11.38	156	138	125	159	158	142

L (ft)	Run 19	20	21	22	23	24
.01	247	245	265	241	265	269
.81	273	273	275	269	281	284
1.64	262	262	264	256	274	277
2.47	271	272	275	268	279	282
3.31	265	266	267	260	276	279
4.14	269	270	273	267	277	280
4.97	261	261	265	257	272	276
5.81	266	268	271	264	275	277
6.64	262	263	266	259	273	277
7.48	261	264	267	259	272	275
8.32	258	259	262	254	270	273
9.14	239	239	239	226	256	258
9.73	243	244	244	230	259	262
10.30	241	244	248	232	260	266
10.63	245	245	245	230	259	264
11.38	186	185	178	155	218	217

TABLE CII (continued)

Measured Wall Temperatures (F)

L (ft)	Run 25	26	27	28	29	30
.01	269	277	277	278	228	228
.81	284	282	282	284	259	261
1.64	277	280	280	283	251	254
2.47	283	280	280	282	257	259
3.31	280	279	279	281	256	257
4.14	281	277	278	279	256	258
4.97	276	276	275	277	247	249
5.81	278	274	274	277	254	256
6.64	277	274	273	276	252	255
7.48	277	273	272	274	251	253
8.32	273	271	271	274	250	251
9.14	259	267	264	267	223	223
9.73	262	268	267	269	229	230
10.30	267	265	266	267	228	228
10.63	266	265	266	268	228	229
11.38	217	243	240	237	160	158

L (ft)	Run 31	32	33	34	35	36
.01	231	234	154	198	229	155
.81	262	263	243	271	280	241
1.64	255	255	258	277	279	258
2.47	261	261	256	276	278	257
3.31	258	259	256	275	277	258
4.14	259	260	253	273	277	254
4.97	251	253	247	269	274	251
5.81	257	258	247	270	275	248
6.64	255	256	251	269	274	251
7.48	255	256	239	266	274	239
8.32	253	254	247	268	274	248
9.14	223	221	247	267	273	246
9.73	230	227	226	261	273	226
10.30	231	230	222	258	270	222
10.63	230	224	238	265	272	237
11.38	154	146	238	262	272	236

TABLE CIII

Steam Pressure (psia)

L (ft)	Run 13	14	15	16	17	18
.01	50.0	52.0	53.0	51.0	49.9	52.3
.81	49.0	51.4	52.5	50.0	49.0	51.8
1.64	48.1	50.9	52.1	49.1	48.2	51.4
2.47	47.1	50.4	51.7	48.2	47.3	50.9
3.31	46.1	49.9	51.3	47.2	46.5	50.5
4.14	45.3	49.4	51.0	46.4	45.8	50.1
4.97	44.4	49.0	50.8	45.5	45.0	49.7
5.81	43.6	48.7	50.6	44.9	44.5	49.4
6.64	42.8	48.4	50.4	44.1	43.8	49.1
7.48	42.3	48.2	50.3	43.6	43.2	48.9
8.32	41.6	48.0	50.2	42.9	42.6	48.7
9.14	41.2	47.9	50.2	42.4	42.2	48.5
9.97	41.0	48.0	50.2	42.3	42.1	48.7
10.30	40.9	48.0	50.3	42.2	42.1	48.6
10.63	40.8	47.9	50.2	41.9	41.9	48.6
11.38	40.7	47.9	50.2	41.8	41.7	48.6

L (ft)	Run 19	20	21	22	23	24
.01	51.9	52.8	55.8	51.0	56.8	60.2
.81	51.0	52.2	55.4	50.8	56.2	59.8
1.64	50.7	51.6	55.0	50.6	55.6	59.4
2.47	49.9	50.9	54.5	50.4	54.9	58.9
3.31	49.2	50.3	54.1	50.2	54.3	58.5
4.14	48.6	49.7	53.6	50.0	53.8	58.1
4.97	47.9	49.0	53.2	49.7	53.1	57.6
5.81	47.3	48.5	52.8	49.5	52.5	57.2
6.64	46.6	47.9	52.5	49.3	51.9	56.8
7.48	46.1	47.4	52.2	49.2	51.4	56.4
8.32	45.4	46.9	51.8	49.1	50.8	56.0
9.14	44.9	46.4	51.6	49.0	50.3	55.7
9.97	44.6	46.1	51.5	49.0	49.9	55.4
10.30	44.5	46.0	51.4	49.0	49.8	55.4
10.63	44.3	45.8	51.3	48.9	49.5	55.3
11.38	44.1	45.6	51.2	48.9	49.1	55.1

TABLE CIII (continued)

Steam Pressure (psia)

L (ft)	Run 25	26	27	28	29	30
.01	61.1	58.1	57.4	60.3	52.2	54.0
.81	60.7	57.5	57.1	60.2	51.2	53.1
1.64	60.4	57.0	56.8	59.9	50.2	52.2
2.47	59.9	56.4	56.3	59.6	49.1	51.2
3.31	59.6	55.8	56.0	59.3	48.2	50.4
4.14	59.2	55.3	55.6	59.1	47.4	49.6
4.97	58.8	54.7	55.2	58.8	46.5	48.8
5.81	58.5	54.2	54.8	58.6	45.8	48.2
6.64	58.1	53.6	54.4	58.3	45.0	47.6
7.48	57.8	53.0	54.1	58.0	44.5	47.1
8.32	57.4	52.4	53.7	57.8	43.8	46.5
9.14	57.2	52.0	53.5	57.5	43.4	46.2
9.97	57.0	51.5	53.2	57.3	43.2	46.1
10.30	56.9	51.4	53.1	57.3	43.2	46.0
10.63	56.8	51.1	53.0	57.2	43.0	45.9
11.38	56.5	50.6	52.7	57.0	42.9	45.8

L (ft)	Run 31	32	33	34	35	36
.01	55.0	57.2	50.2	57.7	58.9	51.6
.81	54.4	56.7	49.7	57.3	58.5	50.7
1.64	53.7	56.1	48.7	56.6	57.9	49.8
2.47	52.7	55.4	47.8	55.8	57.2	48.8
3.31	52.2	54.9	46.9	55.3	57.7	48.0
4.14	51.5	54.4	46.2	54.7	56.2	47.4
4.97	50.9	53.8	45.4	54.1	55.6	46.6
5.81	50.4	53.5	44.8	53.6	55.1	46.1
6.64	49.8	53.2	44.3	53.0	54.5	45.5
7.48	49.5	53.0	43.8	52.5	54.1	45.1
8.32	49.1	52.7	43.4	52.0	53.6	44.7
9.14	48.8	52.6	43.0	51.5	53.2	44.4
9.97	48.8	52.5	42.8	51.1	52.7	44.3
10.30	48.8	52.6	42.8	51.0	52.6	44.3
10.63	48.7	52.6	42.6	50.8	52.4	44.2
11.38	48.7	52.6	42.3	50.4	51.9	44.0

TABLE CIII (continued)

Steam Pressure (psia)

Run	Plenum Chamber Pressure (Saturation)
13	54.1
14	54.4
15	54.7
16	55.0
17	53.5
18	54.4
19	54.7
20	55.4
21	57.6
22	52.1
23	59.2
24	61.9
25	62.6
26	60.3
27	59.0
28	61.5
29	56.6
30	58.0
31	58.6
32	60.1
33	54.6
34	60.5
35	61.3
36	55.4

TABLE CIV

Liquid Film Data

Run 13				Run 14			
h (in)	f (sec^{-1})	Relative contact time (%)	V_w (ft/sec)	h (in)	f (sec^{-1})	Relative contact time (%)	V_w (ft/sec)
.0149	8	0	10.4	.0351	5	0	13.0
.0099	41	0	10.4	.0251	36	8	11.6
.0049	158	7	10.4	.0201	59	11	11.6
.0029	230	21	10.4	.0181	70	15	11.6
.0019	215	33	10.4	.0151	85	18	10.4
.0014	183	43	9.9	.0126	97	18	11.6
.0009	12	73	-	.0101	105	25	10.7
.0007	3	79	-	.0076	105	29	10.4
.0004	0	100	-	.0051	105	42	11.6
				.0031	90	54	9.5
				.0021	56	71	-
				.0016	45	77	-
				.0011	13	88	-
				.0006	3	100	-

TABLE CIV (continued)

Liquid Film Data

Run 15				Run 16			
h (in)	f (sec^{-1})	Relative contact time (%)	V_w (ft/sec)	h (in)	f (sec^{-1})	Relative contact time (%)	V_w (ft/sec)
.0710	9	3	10.4	.0107	7	2	26.0
.0650	12	3	9.9	.0057	56	4	18.9
.0600	18	3	8.7	.0032	116	11	17.4
.0550	22	4	9.5	.0022	158	23	17.4
.0500	31	5	9.9	.0017	176	30	14.9
.0450	39	5	10.4	.0012	198	40	13.9
.0400	47	8	9.5	.0010	204	40	14.9
.0350	51	9	8.7	.0007	173	51	-
.0300	54	15	8.3	.0005	75	79	-
.0250	51	20	9.9	.0004	32	89	-
.0200	49	27	8.3	.0003	14	100	-
.0150	47	33	7.4	.0002	9	100	-
.0100	43	53	9.5	.0001	4	100	-
.0075	38	63	8.3				
.0050	23	80	9.5				
.0040	15	87	-				
.0035	11	93	-				

TABLE CIV (continued)

Liquid Film Data

Run 17				Run 18			
h (in)	f (sec^{-1})	Relative contact time (%)	V_w (ft/sec)	h (in)	f (sec^{-1})	Relative contact time (%)	V_w (ft/sec)
.0106	12	2	20.8	.0515	3	0	17.4
.0096	19	2	23.1	.0415	11	0	17.4
.0086	26	2	20.8	.0365	20	0	17.4
.0076	34	4	18.9	.0315	27	0	13.9
.0066	44	6	18.9	.0265	42	0	13.9
.0056	63	7	18.9	.0215	60	3	13.9
.0046	83	11	17.4	.0165	83	8	12.3
.0036	114	15	16.0	.0115	98	14	11.6
.0026	148	20	16.0	.0090	103	25	11.6
.0016	194	33	14.9	.0065	100	38	12.3
.0011	198	46	-	.0055	100	44	11.0
.0006	137	67	-	.0045	95	53	11.6
.0004	87	93	-	.0035	87	61	-
.0002	23	100	-	.0025	62	77	-
.0001	6	100	-	.0020	44	84	-
				.0015	17	94	-
				.0010	5	100	-

TABLE CIV (continued)

Liquid Film Data

Run 19				Run 20			
h (in)	f (sec^{-1})	Relative contact time (%)	V_w (ft/sec)	h (in)	f (sec^{-1})	Relative contact time (%)	V_w (ft/sec)
.0090	12	0	20.8	.0093	8	5	20.8
.0065	36	0	20.8	.0073	26	8	23.1
.0040	101	5	20.8	.0053	64	12	20.8
.0030	158	9	20.8	.0043	88	13	20.8
.0020	252	17	21.9	.0033	122	18	20.8
.0010	321	35	20.8	.0028	152	20	21.9
.0008	325	41	20.8	.0023	187	25	21.9
.0006	289	50	-	.0018	222	30	21.9
.0005	159	74	-	.0013	254	37	21.9
.0004	104	93	-	.0010	274	45	21.9
.0003	67	100	-	.0008	274	52	-
.0002	20	100	-	.0007	257	55	-
.0001	6	100	-	.0006	206	70	-
				.0005	112	80	-
				.0004	69	100	-
				.0003	29	100	-
				.0002	15	100	-
				.0001	8	100	-

TABLE CIV (continued)

Liquid Film Data

Run 21				Run 22			
h (in)	f (sec^{-1})	Relative contact time (%)	V_w (ft/sec)	h (in)	f (sec^{-1})	Relative contact time (%)	V_w (ft/sec)
.0185	11	0	18.9	.0477	6	0	10.9
.0135	30	2	17.4	.0377	17	0	10.9
.0115	51	3	18.9	.0277	40	1	11.6
.0095	69	5	17.4	.0177	71	5	11.6
.0075	100	8	17.4	.0127	87	12	12.3
.0055	143	12	18.9	.0077	111	21	10.9
.0035	188	25	17.4	.0057	114	30	10.9
.0030	200	28	17.4	.0037	113	47	10.4
.0025	216	33	19.8	.0027	96	58	10.4
.0020	220	42	19.8	.0017	64	79	-
.0015	215	48	17.4	.0007	35	100	-
.0010	75	59	-	.0002	15	100	-
.0005	64	92	-				
.0003	39	100	-				
.0002	17	100	-				

TABLE CIV (continued)

Liquid Film Data

Run 23				Run 24			
h (in)	f (sec^{-1})	Relative contact time (%)	V_w (ft/sec)	h (in)	f (sec^{-1})	Relative contact time (%)	V_w (ft/sec)
.0086	2	0	23.1	.0137	4	0	21.9
.0066	6	2	23.1	.0087	17	0	21.9
.0046	21	2	23.1	.0067	38	0	20.8
.0036	41	4	23.1	.0047	74	4	21.9
.0026	84	8	20.8	.0037	114	5	20.8
.0021	125	10	23.1	.0027	162	12	20.8
.0016	160	12	23.1	.0022	198	16	21.9
.0011	232	22	24.5	.0017	227	19	21.9
.0008	270	34	21.9	.0012	260	26	20.8
.0007	272	36	-	.0011	268	32	20.8
.0006	245	54	-	.0010	270	35	20.8
.0005	162	66	-	.0009	258	37	-
.0004	133	84	-	.0007	198	61	-
.0003	46	100	-	.0006	153	79	-
.0002	14	100	-	.0005	119	86	-
.0001	5	100	-	.0004	77	93	-
				.0003	58	100	-
				.0002	27	100	-
				.0001	14	100	-

TABLE CIV (continued)

Liquid Film Data

Run 25				Run 26			
h (in)	f (sec^{-1})	Relative contact time (%)	V_w (ft/sec)	h (in)	f (sec^{-1})	Relative contact time (%)	V_w (ft/sec)
.0168	4	0	17.4	.0068	2	0	26.0
.0138	12	2	18.9	.0048	11	2	26.0
.0088	45	3	17.4	.0038	21	5	23.1
.0068	77	5	17.4	.0028	49	7	23.1
.0048	119	8	18.9	.0023	75	10	23.1
.0038	150	15	20.8	.0018	135	15	21.9
.0028	189	20	20.8	.0016	106	15	23.1
.0023	214	22	19.8	.0014	137	15	23.1
.0018	235	32	19.8	.0013	162	17	23.1
.0016	244	36	20.8	.0011	178	20	23.1
.0013	242	39	-	.0009	221	22	23.1
.0011	238	47	-	.0008	262	32	23.1
.0008	152	69	-	.0005	281	41	-
.0007	110	80	-	.0004	120	90	-
.0006	93	85	-	.0003	94	100	-
.0005	75	90	-	.0002	42	100	-
.0003	27	100	-				
.0002	18	100	-				

TABLE CIV (continued)

Liquid Film Data

Run 27				Run 28			
h (in)	f (sec^{-1})	Relative contact time (%)	V_w (ft/sec)	h (in)	f (sec^{-1})	Relative contact time (%)	V_w (ft/sec)
.0131	2	0	23.1	.0181	10	0	16.0
.0081	12	2	23.1	.0131	28	0	16.0
.0061	29	2	20.8	.0081	78	3	16.0
.0031	103	7	20.8	.0056	133	8	16.0
.0021	161	10	18.9	.0031	224	15	16.0
.0016	200	14	18.9	.0021	272	24	16.0
.0011	265	19	20.8	.0016	313	32	16.0
.0006	314	40	-	.0011	351	41	16.0
.0005	278	53	-	.0006	333	70	-
.0004	207	69	-	.0001	180	100	-
.0003	153	90	-				
.0002	123	100	-				
.0001	100	100	-				

TABLE CIV (continued)

Liquid Film Data

Run 29				Run 30			
h (in)	f (sec^{-1})	Relative contact time (%)	V_w (ft/sec)	h (in)	f (sec^{-1})	Relative contact time (%)	V_w (ft/sec)
.0192	1	0	23.1	.0193	2	0	24.5
.0142	3	0	20.8	.0143	8	0	24.5
.0092	16	2	20.8	.0093	34	4	21.9
.0072	32	4	23.1	.0073	54	8	20.8
.0052	58	11	23.1	.0063	72	9	21.9
.0042	77	13	23.1	.0053	87	13	20.8
.0032	105	19	23.1	.0043	109	19	21.9
.0022	132	32	21.9	.0033	134	25	20.8
.0012	159	51	20.8	.0030	141	30	20.8
.0011	161	55	21.9	.0028	139	30	18.9
.0010	157	55	23.1	.0023	141	34	20.8
.0009	157	55	-	.0021	150	36	20.8
.0008	154	60	-	.0018	155	38	20.8
.0007	145	68	-	.0017	159	42	20.8
.0006	137	77	-	.0015	163	45	-
.0004	94	100	-	.0013	167	49	-
.0002	79	100	-	.0010	167	57	-
				.0008	160	65	-
				.0006	151	72	-
				.0005	141	76	-
				.0004	22	91	-
				.0003	99	100	-
				.0002	90	100	-
				.0001	82	100	-

TABLE CIV (continued)

Liquid Film Data

Run 31				Run 32			
h (in)	f (sec^{-1})	Relative contact time (%)	V_w (ft/sec)	h (in)	f (sec^{-1})	Relative contact time (%)	V_w (ft/sec)
.0240	4	0	20.8	.0428	2	0	11.6
.0190	11	0	18.9	.0328	12	1	11.0
.0140	31	2	18.9	.0228	38	5	13.9
.0090	79	8	10.4	.0178	60	6	16.0
.0070	104	14	9.9	.0128	95	11	14.9
.0050	134	20	9.9	.0078	136	26	16.0
.0040	152	25	9.9	.0068	139	28	12.3
.0030	166	31	9.9	.0058	151	31	14.9
.0020	176	41	-	.0048	152	39	14.9
.0015	177	53	-	.0038	158	46	-
.0010	167	66	-	.0028	150	51	-
.0005	120	86	-	.0018	136	67	-
.0002	88	100	-	.0008	68	88	-
				.0003	31	100	-

TABLE CIV (continued)

Liquid Film Data

Run 33				Run 34			
h (in)	f (sec^{-1})	Relative contact time (%)	V_w (ft/sec)	h (in)	f (sec^{-1})	Relative contact time (%)	V_w (ft/sec)
.0180	2	0	26.0	.0075	2	0	26.0
.0130	8	2	18.9	.0055	5	4	23.1
.0080	34	4	18.9	.0045	11	8	23.1
.0060	56	8	20.8	.0035	19	12	23.1
.0040	89	17	20.8	.0025	29	15	23.1
.0030	110	23	18.9	.0015	51	23	20.8
.0020	132	35	18.9	.0010	68	38	20.8
.0015	144	42	18.9	.0005	87	61	20.8
.0010	149	52	18.9	.0004	76	81	-
.0005	123	79	-	.0003	71	89	-
.0003	92	100	-	.0002	67	100	-
.0002	85	100	-	.0001	36	100	-

TABLE CIV (continued)

Liquid Film Data

Run 35			
h (in)	f (sec^{-1})	Relative contact time (%)	V_w (ft/sec)
.0080	1	0	23.1
.0045	6	0	23.1
.0035	15	0	20.8
.0025	27	2	20.8
.0020	41	5	20.8
.0015	49	5	18.9
.0010	80	12	20.8
.0005	102	31	-
.0004	95	57	-
.0003	59	81	-
.0001	45	100	-

Run 36			
h (in)	f (sec^{-1})	Relative contact time (%)	V_w (ft/sec)
.0246	2	0	18.9
.0146	17	3	18.9
.0096	51	7	18.9
.0076	75	8	18.9
.0056	105	12	18.9
.0046	125	17	18.9
.0036	140	22	17.4
.0026	160	28	20.8
.0021	170	35	18.9
.0016	181	42	18.9
.0011	181	50	-
.0010	183	53	-
.0009	186	60	-
.0007	169	63	-
.0006	157	73	-
.0005	137	80	-
.0004	121	87	-
.0003	111	100	-
.0001	97	100	-

Appendix D

Calculation of a Statistical Wave Form

The film disturbance layer was first divided into a number of small increments or strips on a common logarithmic scale. The wave frequency and relative contact time corresponding to the graphic midpoint of each increment were determined. A constant velocity over the disturbance layer was assumed to be equal to that of the average measured wave velocity. An average wave density in waves per foot was determined for each strip by dividing the frequency by the wave velocity. The assumption was then made that the experimental relative contact time was the actual percentage of time that the waves were in contact with the probe. Then, dividing the relative contact time by the wave density yielded the wave thickness for a given strip. This calculation is summarized by the following expression.

$$\text{wave width} = \frac{(\text{contact time})\ (\text{wave velocity})}{\text{frequency}} \qquad \text{(D1)}$$

Also, for each strip, the liquid mass flow which occurred in the form of identifiable waves was determined. First, a characteristic strip density was defined as the product of relative contact time and liquid mass density. The mass flow in a strip is then determined from continuity:

$$W = (\text{contact time})\rho_l \pi D_i \Delta h\ V_w \qquad \text{(D2)}$$

where Δh represents the increment width. The results of these calculations are presented in Table DI.

TABLE DI

Statistical Wave Form Calculations

Run	Increment of Disturbance Layer (in)	Mid-Point of Increment (in)	Average Wave Width (in)	Liquid Flow in Waves in Increment (lbm/hr)
13	.0120 - .0076	.0095	.04	1.2
	.0076 - .0048	.0060	.06	6.0
	.0048 - .0030	.0038	.10	10.3
	.0030 - .0019	.0024	.17	12.2
	.0019 - .0012	.0015	.36	13.0
	.0012 - .0008	.0009	1.91	12.6
15	.0700 - .0440	.0550	.16	23.8
	.0440 - .0280	.0350	.22	48.8
	.0280 - .0175	.0220	.46	70.5
	.0175 - .0110	.0135	.86	79.4
	.0110 - .0070	.0088	1.58	69.7
	.0070 - .0044	.0055	3.19	61.5
	.0044 - .0028	.0035	10.00	45.6
18	.0500 - .0280	.0370	.01	.1
	.0280 - .0160	.0210	.09	18.4
	.0160 - .0090	.0120	.30	57.5
	.0090 - .0050	.0066	.64	72.9
	.0050 - .0028	.0037	1.32	68.7
	.0028 - .0016	.0021	3.12	51.7

TABLE DII

Liquid Mass Flow in Identifiable Waves

Run	Liquid Flow Mass in Waves and Sublayer (lbm/hr)	Fraction of W_1 in Waves and Sublayer
13	118	.33
15	344	.96
18	319	.85
23	53	.32
27	69	.48
28	103	.71
29	168	.41

The vita has been removed from the scanned document

A STUDY OF INTERFACIAL WAVES AND HEAT TRANSFER FOR TURBULENT CONDENSATION IN VERTICAL TUBES

by

Oscar Bryan Taliaferro, Jr.

ABSTRACT

A study was made of the film characteristics and the local heat transfer coefficients for the downward flow of steam condensing in a vertical tube. The mass velocity of the steam was such that the flow occurred in the annular-mist regime. The interfacial wave velocities, frequencies, and amplitudes were experimentally determined using needle contact probes. From these data on wave characteristics a statistical wave form was obtained. The liquid mass flow occurring in identifiable waves was determined from a numerical integration over the disturbance layer (i.e., that portion of the liquid layer in which waves are present) and compared to the liquid mass flow given by an energy balance and an entrainment correlation. The results indicated a heavy concentration of liquid particle entrainment in the neighborhood of the film. In addition, the axial profiles of the local heat fluxes and local heat transfer coefficients across the film were obtained. The film Nusselt number at the location of the probes based on an operationally defined mean film thickness was found to correlate with the product of the dynamic quality and the ratio of liquid to gas densities.